

---

# REVIEW OF METHODS FOR AUTOMATIC CEREBRAL MICROBLEEDS DETECTION

---

A PREPRINT

**Maria Ferlin**  
Gdańsk University of Technology  
Gdańsk, Poland  
maria.ferlin@pg.edu.pl

**Zuzanna Klawikowska**  
Gdańsk University of Technology  
Gdańsk, Poland  
zuzanna.klawikowska@pg.edu.pl

**Michał Grochowski**  
Gdańsk University of Technology  
Gdańsk, Poland  
michal.grochowski@pg.edu.pl

**Małgorzata Grzywińska**  
Medical University of Gdańsk  
Gdańsk, Poland  
malgorzata.grzywinska@gumed.edu.pl

**Edyta Szurowska**  
Medical University of Gdańsk  
Gdańsk, Poland  
eszurowska@gumed.edu.pl

February 1, 2023

## ABSTRACT

Cerebral microbleeds detection is an important and challenging task. With the gaining popularity of the MRI, the ability to detect cerebral microbleeds also raises. Unfortunately, for radiologists, it is a time-consuming and laborious procedure. For this reason, various solutions to automate this process have been proposed for several years, but none of them is currently used in medical practice. In this context, the need to systematize the existing knowledge and best practices has been recognized as a factor facilitating the imminent synthesis of a real CMBs detection system practically applicable in medicine. To the best of our knowledge, all available publications regarding automatic cerebral microbleeds detection have been gathered, described, and assessed in this paper in order to distinguish the current research state and provide a starting point for future studies.

## 1 Introduction

Cerebral microbleeds (CMBs) are defined as small, homogeneous, hypointense foci well seen on T2\*-weighted MRI sequences with the associated so-called ‘blooming effect’. They are collections of blood degradation products (mainly hemosiderin) that can remain in macrophages for years, following a microhemorrhage [119, 120, 121, 106]. The ‘blooming effect’ takes place when the MRI overestimates the diameter of the microbleed [12]. CMBs may occur in every region of the brain and can be categorized relative to that area [160, 7, 69], (Fig. 1). They may appear due to a range of pathological processes in the cerebral vessels [121, 9, 8]. Around 5% of population have microbleeds and they are completely healthy [10, 106]. However, the increased number of CMBs in the patient’s brain may indicate the existence of some medical condition [7]. Additionally, they are sometimes accidentally found in association with other pathologies [164]. Undeniably, however, high prevalence of cerebral microbleeds is closely associated with cognitive dysfunction [11].

CMBs detection is a challenging task due to small size of the lesion compared to the whole image (Fig. 2). Moreover, there are many lesions that mimic the CMBs. The main CMB mimics include calcifications, flow voids in pial blood vessels, iron deposits, and deoxyhemoglobin [12]. Both calcium and iron deposits may appear as small foci of low signal intensity on a T2\*-weighted MRI. Flow voids caught in the cross-sections of cortical sulci can be distinguished from CMBs by their sulcal location, equal visibility on T2-weighted SE and GRE sequences, and linear structure when examined over contiguous slices, particularly evident at smaller slice thickness. The presence of paramagnetic deoxyhemoglobin in cerebral venules produces its own blooming effect, which requires the rater to rely on their tubular structure for differentiating them from CMBs. Metastatic melanoma in the brain can appear hypointense on

T2\*-weighted MRI and may mimic CMB. Other mimics, such as mineralization of the basal ganglia or diffuse axonal injury, for instance, can be excluded based on the appearance or clinical history.

CMBs detection is very important considering proper diagnosis and treatment, as they may indicate some major and more complicated issues. From the medical perspective, the crucial information is the number of detected cerebral microbleeds [174, 113, 12, 148]. Another useful information is their location [161, 162, 7, 69, 163]. Therefore, there is no need to perform segmentation which is a complex computational algorithm, it is enough to detect them.

With gaining popularity of the MRI as a good imaging tool, the ability to detect cerebral microbleeds also raises. Unfortunately, for radiologists, it is a time-consuming and laborious process. Technology and automatic image processing can come to the rescue in this case.

Different solutions have been proposed for last years. However, the problem is complex and there is no unification and consistency between the researches. According to our best knowledge, the results achieved so far are still not used in medical practice. In this context, the authors recognized the need to systematize the existing knowledge and best practices as a factor which will facilitate imminent synthesis of a real CMBs detection system, which would be practically applicable in medicine.

The existing research results are in fact difficult to compare due to various, unavailable publicly datasets and the lack of system evaluation metrics. The guidelines included in this paper are expected to present new research in a more beneficial way. Probably, the prevalence of a few publicly available datasets will result in evaluation of new approaches on these datasets.

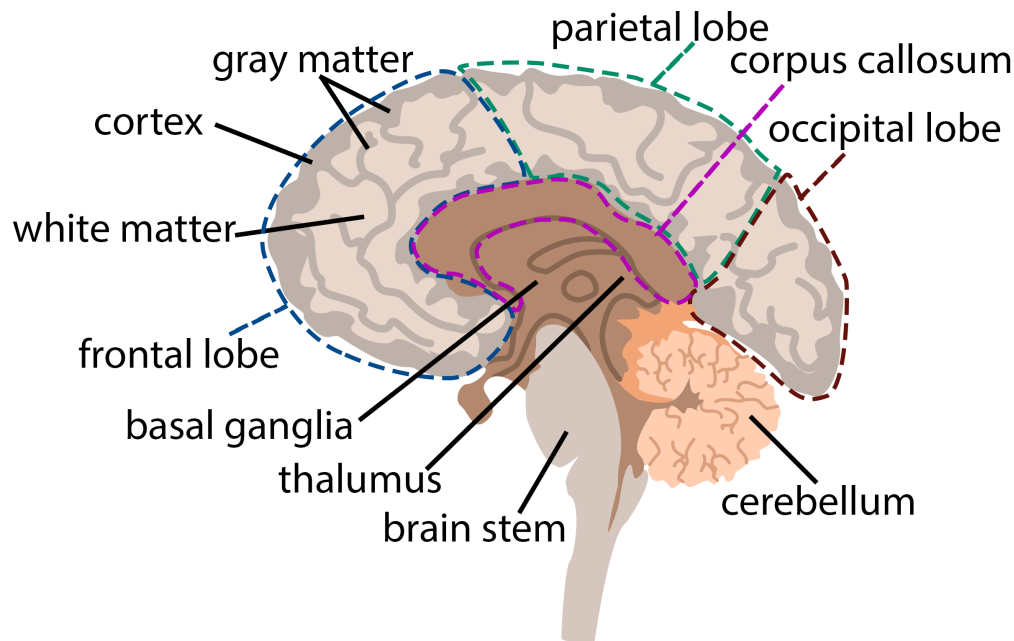


Figure 1: Brain anatomy in the sagittal plane. In addition to the presented structures, the temporal lobe, the insula, and the external and internal capsules, which are not visible in this plane, are also important in the context of scales used to rate CMB. CMBs can be found in all structures indicated in the figure as well as in those mentioned above.

## 1.1 Review criteria

The aim of this research was to gather all previous works and achievements in the field of cerebral microbleeds detection. Regarding the lack of order in existing research and comparison ability we decided to collate different approaches and methods, in order to distinguish the current research state and provide a starting point for future studies. It is noteworthy that the key word in this matter is *automatic* as a guide for a radiologist to detect microbleeds on the MRI existed well beyond [107, 109, 108, 106, 105, 104].

Firstly, a comprehensive literature review regarding automatic cerebral microbleeds detection have been done. In order to do that, careful search was performed for all papers connected with this topic in Google Scholar, IEEE Xplore, and

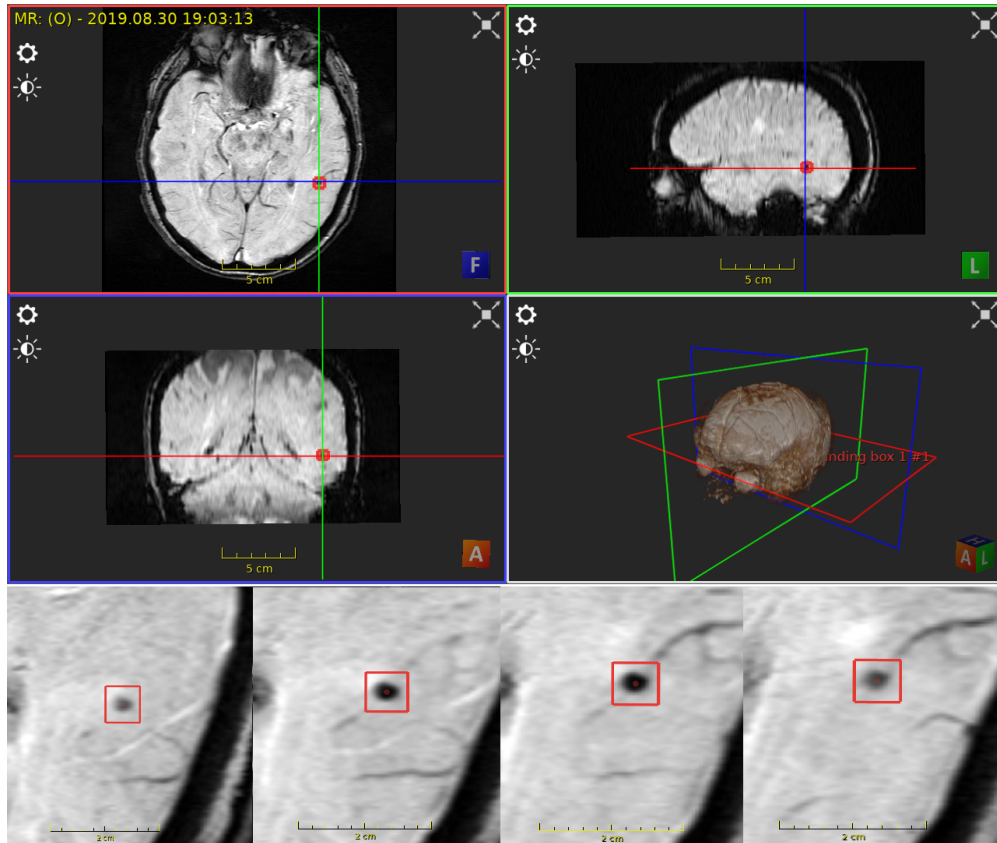


Figure 2: Example of CMB. Upper images present the same microbleed in three planes, while bottom ones present sequence of adjacent slices fragments, in which the microbleed is visible (marked by red frame). Images acquired using ImFusion software.

Elsevier platforms, using key phrases: *automatic cerebral microbleeds detection*, *automatic CMB detection*, *cerebral microbleeds detection*.

The next step was the search for related papers in the references of all gathered works. The literature review dates back to year 2011, in which, to the best of our knowledge, first papers about automatic CMB detection were published.

The main information gathered from each paper referred to: database, pre-processing, methods used, proposed approach with the best or the most significant results, conclusions, and challenges.

For the majority of modern methods, the key issue is the availability of datasets, therefore we decided to collate the information about all datasets used in this type of research in Section 2, which also introduces the issues of MRI and CMB characteristics and CMB rating.

To maintain clarity of the paper, descriptions of particular algorithms are given in Section 3, while the exact approach leveraging from those algorithms is presented in Table 3. The algorithms described in Section 3 are divided into two main groups referring to detection and verification of CMB candidates. Subsection 3.1 also presents different pre-processing algorithms that were used to prepare a dataset for training and testing. Eventually, all methods and algorithms that were used to solve this task are presented. It turned out during the reported research that the evaluation of results is a challenging problem due to the lack of a standard for the metrics used. It is not only problematic for existing approaches comparison, but also makes it impossible to assess a specific method itself. To address this, a range of metrics is presented in Subsection 3.4, along with their features and dependencies.

Section 4 provides a comprehensive assessment of all the presented research, followed by conclusions and challenges, both gathered during literature review and emerging from this analysis.

## 2 Data sources

In order to understand the task of cerebral microbleeds detection it is essential to understand the magnetic resonance imaging, acquisition process and rating procedure. Therefore, we decided to introduce the process of MR images formation. Further, the relevant sequences and rating scales are described. Finally, we present datasets used for cerebral microbleeds detection.

### 2.1 Magnetic Resonance Imaging Sequences

Among the types of brain imaging they are CT (computed tomography) and MRI (magnetic resonance imaging). This paper focuses on MRI because it is the most commonly used technique to study CMB. The main reason is the fact that the CT density of the hemorrhage in CMBs rapidly decreases over days as CMBs become indistinguishable with brain tissue after around 7–10 days [174]. Consequently, the sensitivity of CT in imaging CMBs is the highest within the first few days of their appearance. On MR images, CMBs remain visible much longer than on CT.

MRI is the imaging technique in which each sequence is a combination of radiofrequency pulses and gradients. There are over a hundred different sequence types, the acronyms of which depend on the manufacturer. Regardless of the type of sequence, the goal is to obtain the signal of a particular tissue - contrast, as quickly as possible - speed, while limiting the artifacts and without altering the signal to noise ratio [122].

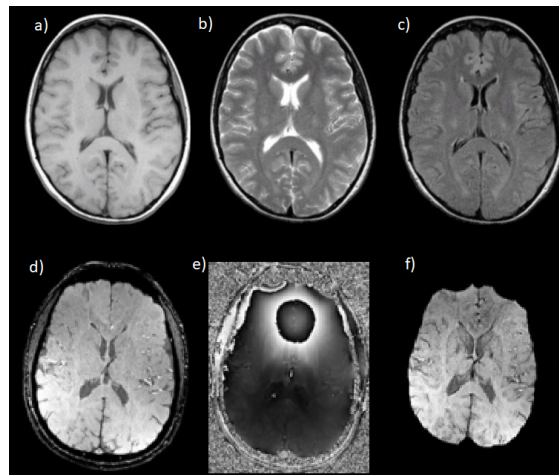


Figure 3: Transverse brain plane. Sequences in first row [118]: T1W (a), T2W (b), FLAIR (c); in second row [117]: Magnitude (d), Phase (e), SWI (f).

There are three essential components for any imaging sequence. The first is the radio frequency (RF) excitation pulse which is required for the phenomenon of magnetic resonance. The second are the gradients for spatial encoding whose arrangement will determine how the k-space is filled. The third component is signal reading, which combines echo types determining the type of contrast - varying influence of relaxation times: T1, T2 and T2\*. Additionally, more sequence parameters, such as repetition time or flip angle, must be chosen to find a balance between contrast, resolution, and speed [147].

There are three types of relaxation times: T1, T2, and T2\* [123]. The term relaxation means that, once the RF pulse is turned off, the spins are relaxing back into their lowest energy state or to the equilibrium state, realigning with the axis of the magnetic field. T1 is called the longitudinal relaxation time, as it refers to the time needed for the spins to realign along the longitudinal (z)-axis. T2 is defined as the predicted time constant for the decay of transverse magnetization arising from natural interactions at the atomic or molecular level. However, in a real MR experiment, the transverse magnetization decays much faster than would be predicted by natural atomic and molecular mechanisms. This accelerated decay rate is denoted as T2\*.

There are two main sequence families, depending on the type of echo recorded. The first family comprises Spin Echo (SE) sequences, which have two essential parameters: TR and TE. They consist of a series of events: 90° pulse; 180° rephasing pulse at half of echo time (TE) and signal reading at TE, repeated at each time interval TR (Repetition Time). During each repetition, the line of k-space is filled due to different phase encoding. The example of such sequence is FLuid Attenuation Inversion Recovery (FLAIR). The second family includes Gradient Echo (GE) sequences,

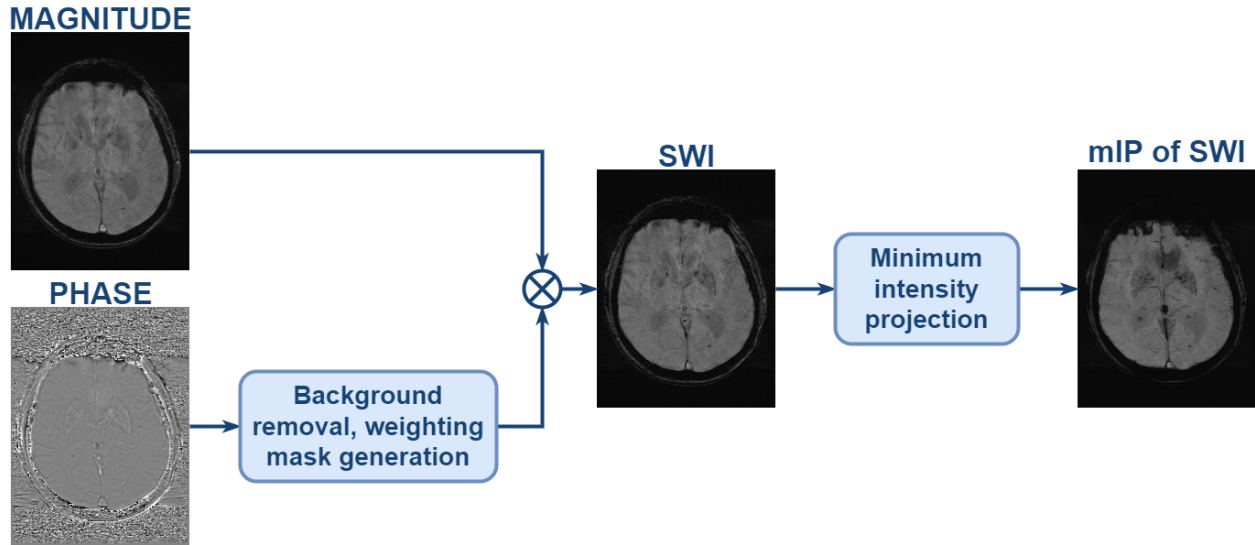


Figure 4: Overview of data processing steps in SWI.

during which the flip angle (FA) is usually below  $90^\circ$ , which decreases the amount of magnetization tipped into the transverse plane. In this case, there is no  $180^\circ$  RF rephasing pulse. The example of this sequence is Susceptibility Weighted Imaging (SWI). Numerous variations have been developed within each of these families, mainly to increase the acquisition speed.

A **T1-weighted** (T1W) sequence demonstrates differences in the T1 relaxation times of tissues. The T1-weighted image is consistent with the anatomy: gray matter is dark and white matter bright. Anatomical gray-white inversion is observed in **T2-weighted** (T2W) images, in which gray matter is bright and white matter dark. It highlights differences in the T2 relaxation time of tissues. Another sequence is **FLAIR**, which removes signal from the cerebrospinal fluid (CSF) in the resulting image. Brain tissue in the FLAIR image appears similar to that in the T2W image with gray matter brighter than white matter, but in this case, CSF is dark instead of bright. **SWI** is a 3D high-spatial-resolution fully velocity corrected gradient-echo MRI sequence which takes advantage of the effect of both phase and magnitude. Fig. 3 shows the described sequences and the data processing steps in SWI are shown in Fig. 4.

Susceptibility weighted sequences are named differently depending on the MRI vendor [170]. For example, the term SWI is owned by Siemens, GE Healthcare offers a sequence called SWAN, and Philips Healthcare has proposed the name SWIp. Obtaining these sequences differs, due to licensing and patent issues [172]. The differences lie in the use of different ways of combining the sequences, e.g. SWI uses phase and magnitude, while SWAN uses a weighted sum of longer TEs, which preserves T2\* dephasing effects, but also increases the signal-to-noise ratio [170, 171]. However, regardless of the vendor SWI-like sequences are most commonly used in CMB detection, as they have greater sensitivity to this lesion than other sequences [111, 39, 34, 40, 112, 113]. It is not only used in terms of automatic detection but also in everyday clinical practice. Another factor that improves the detectability of microbleeds is the strength of the magnetic field [114, 115, 116, 34].

Clinical image data is typically stored in the DICOM format. For scientific analysis, the alternative format is NIFTY.

## 2.2 CMB rating

Technology that automates clinicians' work should be developed in accordance with clinical practice. It is important to know the ways of assessing a disease, so that the results provided by the proposed tools fit into these guidelines. Two ways used by clinicians to assess CMB are **Brain Observer Microbleed Scale** (BOMBS) [7] and **Microbleed Anatomical Rating Scale** (MARS) [69], proposed in 2009. The evaluation categories are presented in Table 1. Standardized CMB rating scales provide a uniform assessment methodology and enable easy and reliable quantification and categorization of CMBs even when the scales are used by observers with different backgrounds or experience, and thus increase the reliability of the measurement.

Measurement reliability refers to the consistency or repeatability of the measurement. Low reliability indicates large differences in measurement while retesting. It precludes reproduction or interpretation of the results, and finally makes

Table 1: CMBs evaluation categories according to rating scales

BOMBS	MARS
<ul style="list-style-type: none"> <li>• certainty:               <ol style="list-style-type: none"> <li>1. certain,</li> <li>2. uncertain,</li> </ol> </li> <li>• size:               <ol style="list-style-type: none"> <li>1. &lt;5 mm,</li> <li>2. 5-10 mm,</li> </ol> </li> <li>• side of brain:               <ol style="list-style-type: none"> <li>1. left,</li> <li>2. right,</li> </ol> </li> <li>• location (Fig. 1):               <ol style="list-style-type: none"> <li>1. lobar:                   <ol style="list-style-type: none"> <li>(a) cortex/gray–white junction,</li> <li>(b) subcortical white matter,</li> </ol> </li> <li>2. deep:                   <ol style="list-style-type: none"> <li>(a) basal ganglia,</li> <li>(b) internal and external capsules,</li> <li>(c) thalamus,</li> </ol> </li> <li>3. posterior fossa:                   <ol style="list-style-type: none"> <li>(a) brain stem,</li> <li>(b) cerebellum.</li> </ol> </li> </ol> </li> </ul>	<ul style="list-style-type: none"> <li>• appearance of the lesion:               <ol style="list-style-type: none"> <li>1. definite,</li> <li>2. possible,</li> </ol> </li> <li>• side of brain:               <ol style="list-style-type: none"> <li>1. left,</li> <li>2. right,</li> </ol> </li> <li>• location (Fig. 1):               <ol style="list-style-type: none"> <li>1. lobar:                   <ol style="list-style-type: none"> <li>(a) frontal,</li> <li>(b) parietal,</li> <li>(c) temporal,</li> <li>(d) occipital,</li> <li>(e) insula,</li> </ol> </li> <li>2. deep:                   <ol style="list-style-type: none"> <li>(a) basal ganglia,</li> <li>(b) internal capsule,</li> <li>(c) external capsule,</li> <li>(d) thalamus,</li> <li>(e) corpus callosum,</li> <li>(f) deep and periventricular white matter,</li> </ol> </li> <li>3. infratentorial:                   <ol style="list-style-type: none"> <li>(a) brain stem,</li> <li>(b) cerebellum.</li> </ol> </li> </ol> </li> </ul>

distinguishing between participants with and without specific medical conditions impossible due to significant measurement error. In clinical evaluation, a measurement error can be introduced by the observer. Therefore, determining observer (clinician) reliability is important for making full comparison of measurement reliability between studies. There are two ways of doing it – inter- and intra-observer agreement.

**Intra-observer** agreement determines the degree of agreement between the two studies that use the same technique, in the same patient, obtained by the one observer [110]. **Inter-observer** agreement determines the degree of agreement between the two studies that use the same technique, in the same patient, obtained by the two observers [110].

The reliable rating of CMBs presence, number, and location is the important factor for further diagnosis of various diseases. However, many research institutions use their own methods to rate CMBs. Although their reliability based on intra- and inter-observer agreement is reported, details of the methods used are usually not described [109].

Table 2: Comparison of dataset acquisition parameters used in the reviewed approaches.

ref.	# of subject /# of CMB	RES [mm <sup>2</sup> ]	ST [mm]	TR [ms]	TE [ms]	FA [°]	BW [Hz/px]	IMS [voxels]	FOV [mm <sup>3</sup> /mm <sup>2</sup> ·mm]	Sequences	$\beta$ [T]	Rating	Avail.
[32]	2/4	0.35x0.35	0.3	20	2.5/15	-	-	-	-	T2*W	7	MARS	on request
[25]	6/26	0.5x1	2	57	40	20	-	512x320x48	-	Fully Flow-Compensated 3 DGRE	1.5	[173]	-
[14, 77, 23]	10/-	0.5x0.5	2	-	20	15	120	364x448x48	-	SWI	3	MARS	-
[26, 51]	15/420	0.5x0.5	2	56	28	20	-	u x u 40	240	T2*W	3	similar to BOMBS/MARS	10 subjects
[33]	18/54	0.35x0.35 T2*W, 0.66x0.66 T1W	0.3 T2*W, 0.7 T1W	20 T2*W, 7 T1W	2.5/15 T2*W, 3 T1W	-	-	-	-	T2*W, T1W turbo field echo	7	MARS	on request
[75, 49], [46, 47, 48], [20, 4, 53]	20/-	0.5x0.5	2	28	20	15	120	364x448x48	-	SWI	3	MARS	-
[138]	20/-	0.45x0.45	2	17	24	-	-	-	-	SWI	3	-	-
[42, 24], [18, 76], [43]	20/117, 44/615, 320/1149	0.45x0.45	2	17	24	-	-	512x512x150	230x230	SWI	3	MARS, MARS	20 subjects
[6]	24 / >157	1x1	1	T1W-MPRAGE (T1WMP), 3200 T2W, 35 SWI	2.93 T1WMP, 408 T2W, 7.5/15/22.5/30 SWI	9 T1WMP, 120 T2W, 1.5 SWI	170 T1WMP, 750 T2W, 200 SWI	256x256x176 T1WMP & T2W, 256x192x96 SWI	-	T1WMP, T2W, SWI	3	Inspired by BOMBS	on request
[126]	26/-	-	3	-	-	-	-	u x u x 40-60	-	SWI	-	-	-
[44]	26/404	1x1 T1W-MPRAGE (magnetization prepared rapid gradient echo)	2 SWI, 1 T1W-MPRAGE	-	25	-	-	-	-	SWI, T1W-MPRAGE	3	-	-
[41]	30/64, 41/103, 66/231	0.93x0.93 SWI, 1x1 T1W	1.75 SWI, 1.2 T1W	27 SWI, 2.3 T1W	20 SWI, 2.98 T1W	20 SWI, 9 T1W	-	-	240x256 T1W,	SWI, T1W	3	MARS, MARS	on request
[29, 45]	51/627	0.98x0.98 SWI, 1x1 T1W-MPRAGE (T1MPR)	-	27 SWI, 2300 T1MPR	20 SWI, 2.98 T1MPR	15 SWI, 9 T1MPR	120 SWI, 240 T1MPR	-	-	SWI, T1-MPRAGE	3	MARS	-

Table 2: **Continued:** Datasets acquisition parameters comparison

[19]	58 / 1301	-	5 T2F & T2WF, 2 SWAN-W	5727 T2 PRFSE (T2F), 77.3 SWAN-W, 8400 T2W FLAIR (T2WF)	93 T2F, 45 SWAN-W, 145 T2WF	15 SWAN-W, 145 T2WF	833 T2F & T2WF, 625 SWAN-W	512x512 x u	240	T2F, SWAN-W, T2WF	3	-	-
[2]	72 / 64	0.43x0.43 T2*W SWI, 0.43x0.43 T2*W GRE	1 T1W, 2 T2*W SWI, 1 T2*W GRE	6.6 T1W, 17 T2*W SWI, 15 T2*W GRE	3 T1W, 24 T2*W SWI, 22 T2*W GRE	-	-	-	256x200 T1W, 244x197 T2*W SWI, 220x181 T2*W GRE	T1W, T2*W SWI, T2*W GRE	3	[12]	on request
[35]	72 / 148	0.96x0.96 T2*W & FLAIR, 1x1 T1W	3 T2*W & FLAIR, 1 T1W	1653 T2*W, 11000 FLAIR, 7.9 T1W	20 T2*W, 125 FLAIR, 4.5 T1W	-	-	-	-	T2*W, FLAIR, T1W turbo field echo	3	MARS	on request
[1, 30], [18]	72 / 188 HR, 107 / 572 LR	0.50x0.50 HR, 0.80x0.80 LR	2	27 HR, 40 LR	20 HR, 13.7 LR	15	120	512x448x72 HR, 256x224 HR, 288x252x72 LR 201x229 LR	SWI, Phase, Magnitude	3	[12]	no	no
[17]	73 / 2835	0.5x0.5	1 SWI, 2 3DSPGR	40 SWI, 50 3DSPGR	2.4/12/14.3/20.3 SWI, 16 3DSPGR	25	-	512x512 x u	-	4-echo 3D TOF-SWI, 3DSPGR (3D Spoiled Gradient Recalled)	7	computer- aided detection developed by [26] with rater	-
[73]	74 / -	0.938x0.938	5	T2W Fast Spin Echo (T2WFSE), 300 T2*GRE	105 T2WFSE, 40 T2*GRE	20	-	256x224x u T2WFSE	240x180	T2WFSE, T2* GRE	1.5	MARS	on request
[13]	186 / 1716	0.63x0.63	2	1050	20	21	-	-	220x198	3D Fast Field-Echo	3	-	-
[74]	214 / 235	0.93x0.93 SWI, 1x1 T1W	1.75 SWI, 1.2 T1W	27 SWI, 2.3 T1W	20 SWI, 2.98 T1W	20 SWI, 9 T1W	-	u x u x 160 T1W	240x256 T1W	SWI, T1W	3	MARS	on request
[5]	220 / 1011	0.45-0.53x 0.57-1.05 1.5T, 0.50-0.54x 0.50-1.07 3T	2-2.65 1.5T, 2/2.3 3T	49/50 1.5T, 27-34 3T	40 1.5T, 17.5-20 3T	15 1.5T, 12/15 3T	80 1.5T, 100-425 3T	304-448x 56/60 1.5T, 448-512x 322-416x 56/128 3T	-	-	1.5/3	-	on request
[21]	237 / 631	0.5x0.5	1.6 T2*W, 0.8 GRE PDW	-	-	-	-	-	-	3D T2*W, GRE Proton- Density Weighted	1.5	-	-
[20]	270 / >505	0.9x0x8 T2*-GRE, 0.8x0.8 SWI	5 T2*-GRE, 3 SWI	504 T2*-GRE, 27 SWI	15 T*2-GRE, 9.4/20 SWI	-	-	640x640x28 T2*-GRE, 256x288x48 SWI	-	T2*-GRE, SWI	-/3	MARS	on request
[72]	320 / 114 SWI, 179 / 760 SVS	0.45x0.45 SWI	2	17 SWI, 27/40 SVS	24 SWI, 20/14 SVS	15 SVS	120 SVS	512x512x150 SWI	230x230 SWI	SWI	3	MARS SWI/ [12] SVS	-



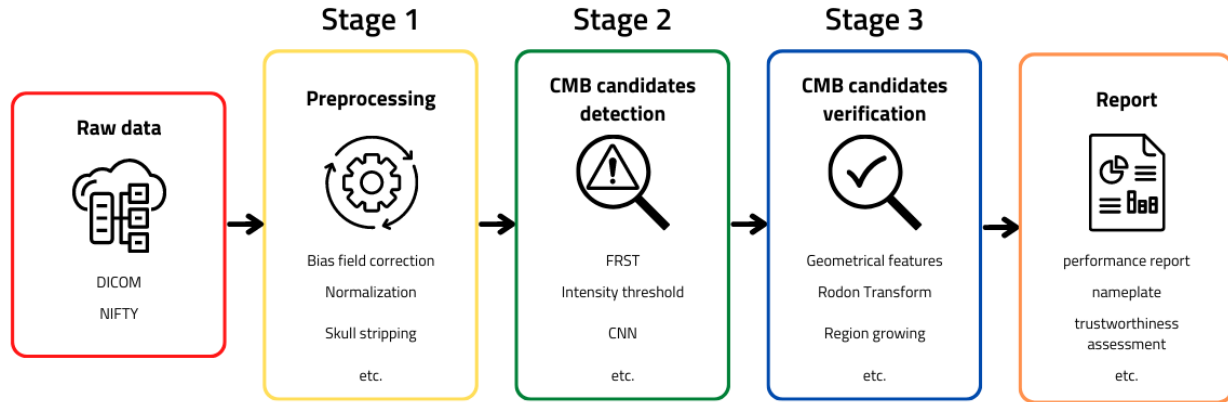


Figure 5: Pipeline of a typical CMB detection approach.

### 2.3 Datasets

Studies on the tools that automatically detect microbleeds can be divided into three categories based on the source of the data used. The first category includes researches that use data from specific, existing studies: [25, 2, 41, 28, 27, 21, 78, 32, 33, 35, 5, 74, 34, 6, 20]. The second category refers to studies that collected data specifically to develop this tools: [1, 30, 26, 51, 17, 42, 43, 3, 80, 79, 24, 18, 14, 77, 23, 35, 19, 31, 76, 22, 75, 49, 73, 72, 46, 47, 48], whereas the third category contains studies that do not specify the sources of data used: [52, 45, 29, 13, 44, 53, 4, 50, 126, 124, 125, 138, 137, 140, 139]. The researches focused on diagnosing several medical conditions: Alzheimer’s and elderly diseases (AD) [25, 2, 41, 28, 27, 21, 78, 35, 74], Cerebral Autosomal Dominant Arteriopathy with Subcortical Infarcts and Leukoencephalopathy (CADASIL) [52, 14, 77, 23, 75, 49, 53, 4, 50, 46, 47, 48, 124, 125, 139], Second Manifestation of Arterial Disease (SMART) [32, 33], Traumatic Brain Injury (TBI) [45, 29, 5, 44, 140], stroke [31, 5, 73, 20], Intracerebral Haemorrhages (ICH) [34, 20], gliomas [26, 51, 17], hemodialysis cases [5], Cerebral Amyloid Angiopathy (CAA) [34], atherosclerosis [6], or did not distinguish any particular disease besides the appearance of CMBs [1, 30, 42, 43, 3, 80, 79, 24, 18, 19, 76, 22, 13, 72, 20, 126, 138, 137]. Datasets used in the first category of researches focused on AD [81, 82, 83, 36, 84, 85], SMART [37], TBI [86], stroke [86, 89], ICH [87, 90, 91], gliomas [70], hemodialysis cases [86], CAA [88], atherosclerosis [38], or CMBs [92].

Clinicians rated the CMBs present in the images from these datasets according to the MARS scale, the BOMBS scale, or an unspecified standard. Details related to the number of patients, image acquisition parameters, types of sequences, strength of magnetic field and data availability are given in Table 2. The abbreviations used in the table stand for: RES – resolution, TR – repetition time, TE – echo time, FA – flip angle, BW – bandwidth, IMS – image matrix size, ST – slice thickness, FOV – field of view, u – unknown dimension.

Datasets that were not included in the table due to insufficient information are [137, 140, 124, 125, 52, 139, 22, 78]. They contained only information about, for example, the number of patients or the type of sequence.

## 3 Methodology

A comprehensive analysis of the past works regarding cerebral microbleeds detection has led to the proposition of a generalized pipeline of such a system. The majority of works can be divided into three stages: *Pre-processing*, *CMB Candidates Detection* and *CMB Candidates Verification*. Therefore, we decided to describe the methodology having regard to such division. The overall idea is presented in Fig. 5. All the methods and algorithms available within each stage are firstly described as single transform, that can be applied. Their further synthesis into a complete approach along with the paper in which it was used are in Table 3.

### 3.1 Pre-processing

Data pre-processing is an important step in system synthesis. Proper preparation of data has a significant impact on further system performance.

It is important to understand that phrase *raw data* does not always mean that data were not pre-processed by MRI software. From the system’s perspective, raw data are those provided by the MRI. However, there is a variety of MRI

device suppliers, who design an operating system of their own, which performs different operations on a particular scan before the image delivery. Therefore, it is crucial to know how the data has already been processed and what else can be improved to meet system needs.

Below the most popular types of operations performed on raw data are presented and few examples illustrated in Fig. 6. Firstly, there are operations for removing artifacts and unnecessary information.

**Bias field correction** is the operation that reduces negative influence of the bias field, which is an undesired artifact in most MRI images, especially old ones. It can also be called **intensity inhomogeneity correction**. The most commonly known techniques include N3 Bias Correction [60] and its successor N4ITK/N4 [59], FSL FAST [65] or reconstruction Syngo MR B17 provided by the manufacturer. Nevertheless, there are also other methods for bias field correction [93, 16]. This operation was applied by [21, 28, 27, 44, 45, 46, 29, 5, 125, 6, 74, 20]. **Skull stripping** also known as **brain extraction** is an operation of removing skull and background from the image, leaving only the brain. There are plenty of algorithms for performing this task: Brain Extraction Tool (BET) [56], BrainSuite [57], and others [98, 97]. Brain extraction was applied in [32, 25, 21, 26, 28, 44, 45, 29, 24, 51, 17, 1, 30, 2, 13, 138, 20].

**Normalization** is a typical operation of rescaling the pixel values into range (0,1) or (-1,1). This enables bias reduction in the next stages of system creation. It was applied by [32, 73, 25, 33, 35, 26, 41, 28, 27, 42, 43, 45, 5, 6, 18, 72].

**Standardization** is an equally common operation as normalization and involves subtraction of mean value of pixels and division by the standard deviation of them. It was claimed to be used in [32, 33, 35, 18].

**Mask generation** is a wide term as different types of masks might be generated. The most common is binary mask that might be generated using Statistical Parametric Mapping Toolbox [95] or morphological operations [100, 99]. Further, there are typically neurological masks such as cerebrovascular fluid (CSF) mask, gray-white matter (GWM) mask and white-matter (WM) mask. Masks were generated in [32, 73, 33, 35, 26, 41, 28, 27, 45, 29, 78, 17, 126, 23, 76, 2, 72].

**Further image generation** involves using images provided by the MRI device to make a new image consisting more information. For instance, a SWI sequence is generated from the Magnitude and Phase sequences. These days, it is the standard sequence generated by the scanner. Further, the SWI data might be processed using [103] for phase enhancement, like in [44] Similarly, T2\*-weighted images are nowadays provided by the MRI scanner, but in the past they had to be obtained from PD-weighted images using, for example, Elastix Tool [61]. It was performed for example in [21, 5, 17]. A QSM image can be generated using Morphology Enabled Dipol Inversion (MEDI) [64], like in [6].

**Slice merging** can also be considered as a new image creation, which involves concatenation of adjacent slices to provide 3D information. Generally, MRI images are one-channel. It enables putting three adjacent slices into one image using RGB channels. The concatenation of different sequences of corresponding slices might be done as well. However, in this case it may be necessary to align the slices with each other, if there were different parameters of acquisition. This kind of operation was performed in [3, 1, 30, 18].

Useful software to perform these operations is Neuroimaging Core [94] involving Advanced Normalization Tools (ANT), FMRIB Software Library (FSL) [55, 66, 67, 127] and Statistical Parametric Mapping (SPM). The last software is also implemented in [95] based on [96].

There are also some typical transforms performed in standard image pre-processing. It is noteworthy that medical data are highly sensitive to any transformation, after which significant information can be accidentally lost.

**DICOM to JPG conversion** is an excellent example of lossy data conversion technique, which might influence further processing stages. It was done by [19]. Although DICOM or NIFTY formats might be considered not developer-friendly, working on original image matrices should be a standard.

**Resize** is a common operation of changing image size. It is usually performed to obtain equal sizes of all images, or to enlarge images so that the objects were more visible. It can also be forced by requirements of a method used in the *CMB Candidates Detection* stage. The images were resized in [25, 5, 2, 18].

**Padding** is performing an artificial size change by addition of a black frame to obtain a desired image size without applying resize. It was utilized by [6, 18, 72].

**Image cut** is a common operation performed to simplify the detection task. It involves image partitioning into smaller parts and then feeding them into the classifier. It might be performed using the sliding neighborhood processing (SNP) technique to produce smaller fragments of the original image. A lot of works utilized this method: [46, 22, 53, 48, 47, 52, 139, 4, 14, 77, 23, 124, 125, 75, 49].

**Rotation** is a simple operation of changing image orientation. However, it can be a loss operation, and therefore a rotation with original intensity should be considered, like in [20], for instance by using `-fslreorient2std` tool [127].

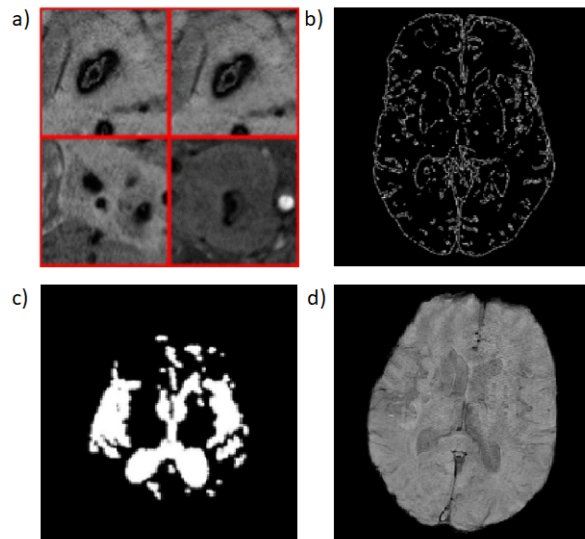


Figure 6: Example of pre-processing operations: a) sliding neighborhood processing [23], b) Canny edge detection [2], c) CSF mask [13] d) brain extraction using BrainSuite software.

**Inversion** is the operation which consists of swapping intensity values in relation to the center of the intensity interval and it was performed by [27].

Finally, there is **data augmentation**, which is not always considered as a pre-processing technique, but rather a regularization one. However, it is sometimes performed at this stage and consists of image transformations, therefore it is placed in this section. It enhances a dataset, especially in case of small amount of data by creating new, slightly modified, artificial images. There is a wide range of transformations, including those described above, along with blur, crop, etc. [135, 101, 102]. Augmentation was used in [140, 78, 124, 6, 13, 19, 18, 74, 138].

### 3.2 Algorithms for CMB candidates detection

Over the years, a wide range of algorithms were used to detect cerebral microbleeds, starting from the simplest methods based on traditional image transformations, up to complicated deep learning models.

#### 3.2.1 Classical methods

In early works regarding CMBs detection the candidates were extracted using predetermined features such as: **intensity threshold** and **area size** [25, 21, 42, 43, 24]. In the SWI sequence CMBs occur as low-intensity spheres, therefore applying a proper intensity threshold allows for **binary mask** generation. Sometimes the authors also applied morphological operations such as **filtering**, **hole filling**, etc. [73, 24, 138]. However, this kind of operations were used at all the stages described in this paper, as they were also useful for *CMB candidates verification*. Next, the detecting procedures evolved to include more complicated voxel features, such as: **eigenvalues** in [20] – scalars associated with the given linear transformation, **line detection** in [41] – defining the line where edge points are located, **Gaussian filter** in [20] and **Laplacian of Gaussian** operator in [28, 27, 20], which highlight the rapid change of the image intensity, **Hough transform** in [2] that enables shape detection by finding objects - local maxima, **Canny filter** in [2] which enables edge detection **watershed transform** in [137] - transforming images to grayscale topographic like map, and distinguishing objects on the basis of its intensity value or **Frangi filters** in [20] - a dedicated filter enabling vessel distinction, or 3D gradient co-occurrence matrix (3D GCM) in [72], which indicates the differences between intensity of two adjacent pixels.

Simultaneously, the researchers began to use the Radial Symmetry Transform (RST), and its successor Fast Radial Symmetry Transform (FRST) [54]. This algorithm deserves special attention since it is successfully used to this day [32, 33, 35, 26, 51, 5, 17, 20]. In this transform, a gradient of the image is computed, then the orientation and magnitude of each pixel is established. Next, using the above values, points of interest can be selected according to the given formula. This algorithm was later developed so that it could be used in 3D space. However, despite its common use, when applied to candidates detection, FRST generates a lot of false positives, which forces introducing the third stage to the whole detection procedure.

Another algorithm used in the *CMB Candidates Detection* stage by [44] was the **region growing** that inspects the homogeneity of the considered pixel - or voxel in case of 3D [165].

### 3.2.2 Neural networks-based methods

Then, with the development of neural networks (NN), algorithms based on these networks gained more attention. Generally, two approaches for neural networks usage may be distinguished: custom or general purpose pretrained neural network. In the first case, in the domain of CMBs detection various approaches were used, such as: simple **artificial neural networks** (ANN) [155] used in [48, 74], which is basically a sum of inputs multiplied by weights assigned in the training process, **back-propagation neural networks** (BPNN) [166] utilized in [139] that are ANNs extended with the information about the error, **sparse auto-encoder** (SAE) [167] used in [46, 47] that is a neural network consisted of encoder and decoder with the additional sparsity penalty algorithm.

The **Random Forest algorithm** [68] was used as well in [45, 29]. It is a black-box algorithm that consists of an ensemble of classifiers that predict an output value based on a part of a dataset and then these predictions are averaged into one.

Finally, there are **convolutional neural networks** (CNN) [168], which are the most popular solution [22, 53, 78, 77, 23, 124, 75, 49, 72].

Basically, CNN consists of a number of feed-forward convolutional layers, where the features are extracted by performing a convolution with predefined filters on every image and then further modified during training. Each convolution layer is followed by a non-linear activation function. Consecutive convolution layers are interspersed by pooling layers that extract the most important features. Then, mostly, there is a fully connected layer or other classifier that assigns a predicted class based on the previously extracted features. An interesting approach is replacement of a fully-connected layer by Extreme Learning Machine [128], which is much more efficient [49].

In the second approach, one takes advantage of a deep neural network architecture that has already been trained on a vast dataset – transfer-learning – often very different from terminal one and just adjusts it to the considered problem. These networks usually consist of millions of parameters and are hard to train on the CPU due to hardware limitations. Additionally, it is a good method for dealing with small dataset problem. The transfer-learning idea is to use a pre-trained network that has already learned some image features and fine-tune it on the particular dataset. Several networks were used for this purpose, including: AlexNet [131] in [126], ResNet50 [15] in [14], Faster-RCNN [129] in [18], VGG [132] in [125], U-Net [63] in [6], YOLOv2 [130] in [1, 30], DenseNet 201 [133] in [4] or SSD [62] in [19] with the modification of feature enhancement. Sometimes, especially in case of SNP algorithm usage the detection task was substituted by classification of small fragments of image using either CNN or ResNet50 for instance in [14, 77]. Considering the main aim of this paper, the description of each network is omitted, as they are explained in detail in the mentioned papers. Nevertheless, the reader is strongly encouraged to get familiar with these architectures.

Relatively new and still not fully explored architectures are **3D convolutional neural networks** (3D CNN). The idea is the same as in 2D CNNs, but instead of performing convolution on 2D matrices, it is performed on 3D patches. They were applied in [3, 140].

### 3.3 Algorithms for CMB candidates verification

Due to the nature of the considered problem, most of the presented approaches involved the *CMB Candidates Verification* stage. In spite of this, some solutions still have not managed to acquire satisfying quality.

In some cases, the process of false positive candidates elimination was performed manually by a radiologist [32, 25, 33, 35, 51, 17, 2]. Although this kind of approach significantly reduced the time needed for one scan rating, it is a semi-automated one.

A large part of the research involved at this stage establishing a batch of predefined features of CMB : from simple ones as intensity or size, to very complicated parameters of a single voxel, calculated in 2D or 3D spaces. There were also other methods for defining the feature vectors, for instance 2D CNN in [42, 138], 3D ISA network [152] in [43], 3D Radon Transform [153] in [28, 27] or feed-forward feature selection (FFFS) [154] in [21].

In some cases, thresholds of geometric features were set, and on this ground the classification was performed [26, 44, 70, 2, 20].

In others, these features together with the previously prepared fragments of images were passed to the classifier. A lot of classifiers have already been tested: Supported Vector Machine (SVM) [58] in [25, 42, 43, 24], linear criterion

classifier (LDC) [134], quadratic discriminant classifier (QDC) [151], Parzen classifier [150] in [21] and Random Forrest Classifier (RFC) [68] in [28, 27].

A common approach at this point was also using a previously generated CSF mask to distinguish a real CMB from vessels, and a WM mask to include the information about the location of potential microbleed [26, 2, 13].

Another approach utilized the advantage of a 3D CNN. It was usually performed for 3D information inclusion, resulting with FP reduction, after the 2D algorithm used in the *Candidates detection stage* [169] [3, 5, 17, 1, 30].

Some works present also usage of region growing algorithm for CMB verification [26, 29, 70].

There was also an algorithm investigating the overlap between predictions from adjacent slices [18]. It not only enabled removal of false positive predictions that were in fact a ground truth, although labeled in the adjacent slice, but also helped finding a real CMB that was detected in the adjacent slice in spite of the previous false negative prediction.

### 3.4 System output and evaluation

To comprehensively validate the quality and robustness of the system, one should take advantage of a number of commonly accepted metrics that provide complementary insight into various aspects of system performance.

A common oversight is to not include metrics that are complementary and provide a view of the system as a whole, not just a part of it. For instance, the sensitivity metric is useless alone, as it can be artificially inflated. It is necessary to provide the precision or F1 score value to properly interpret the sensitivity. In addition, the lack of a uniform way of result evaluation makes it impossible to compare approaches and effectively assess their usefulness.

The evaluation should be performed on a separate dataset or at least separate subjects, using, for instance, cross-validation to avoid randomness.

There are different metrics regarding the type of solved problem. For classification evaluation, the most popular metrics are accuracy (1), precision (4), sensitivity/recall (2), and F1 score (5) that combines precision and sensitivity.

In the case of detection and segmentation, more detailed metrics are required as not only a proper class is important, but also the overlapped area of ground truth label and prediction. In that case, the average precision (7) metric is used, and it is calculated for different values of IoU (6).

The CMBs detection task is known to produce large number of false positive predictions. Therefore two additional metrics were provided particularly for this problem, namely it is FPavg (8) and FPcmb (9).

The mentioned metrics are calculated as follows:

$$\text{accuracy} = \frac{TP + TN}{TP + TN + FP + FN} \quad (1)$$

$$\text{sensitivity} = \frac{TP}{TP + FN} \quad (2)$$

$$\text{specificity} = \frac{TN}{TN + FP} \quad (3)$$

$$\text{precision} = \frac{TP}{TP + FP} \quad (4)$$

$$\text{F1 score} = 2 \times \frac{\text{sensitivity} \times \text{precision}}{\text{sensitivity} + \text{precision}} \quad (5)$$

$$\text{IoU} = \frac{\text{Overlap area}}{\text{Union area}} \quad (6)$$

$$\text{AP} = \int_0^1 p(r) dr \quad (7)$$

$$\text{FPavg} = \frac{FP}{n} \quad (8)$$

$$\text{FPcmb} = \frac{FP}{m} \quad (9)$$

where:

- $TP$ —true positive – the number of actual CMBs detected;
- $FP$ —false positive – the number of predicted CMBs that were not marked as CMB in ground truth;
- $FN$ —false negative – the number of actual CMBs not detected;
- $IoU$ —intersection over union;
- $r$ —recall (sensitivity);
- $p(r)$ —precision as function of recall;
- $n$ — number of subjects (patients) in the test set;
- $m$ — number of CMBs in the test set.

Accuracy (ACC) (1) shows how the system deals with the classification in general. A high score means that almost all labels have been properly assigned.

Sensitivity/recall (2), also known as true positive rate (TPR), shows how the system deals with the ground truth detection or classification. A high score means that almost all ground-true samples have been determined.

Specificity, also known as true negative rate (TNR) (3), discloses the system ability to recognize the negative class.

Precision (4), or positive predictive value (PPV), informs whether the prediction matches ground truth. A high score means that the system generates a small number of false positives.

F1 score (5) helps to check whether there is a balance between sensitivity and precision.

IoU (6) stands for Intersection over Union and shows the common area between prediction and ground truth. It is actually a special case of geometrically oriented Jaccard Index [71]. The average precision (7) AP@0.5 represents the area under the precision-recall curve with IoU of 0.5 and it is used in detection and segmentation. There is also an AUC - area under curve - metric. In case of classification it refers to the ROC curve - sensitivity as a function of 1-specificity.

FPavg (8) shows the average number of false positive predictions per subject, while FPcmb (9) is the number of false positive predictions per one ground truth sample. For example, when we have one subject with 5 ground truth CMBs and 1 false positive prediction. The FPavg will equal 1 and FPcmb will equal 0.2.

Table 3: Comparison of existing approaches<sup>1</sup> The most promising ones are marked with bold.

Reference	Pre-processing	First stage	Second stage	TPR	PPV	F1	FPavg	FP/CMB	TNR	ACC
Kuijf et al., 2011, [32]	SPM8, BET, standardization	3D RST	manual inspection	-	-	-	5*	-	-	-
Seghier et al., 2011, [73]	SPM8, normalization	CSF, GWM, CMIBs, skull scalp, background img	morphological operations (2 iterations)	Authors did not provide any metric, only the table of results for each case.						
Barnes et al., 2011, [25]	brain extraction, resize, normalization	intensity histogram threshold	SVM, manual review	81.7	-	-	107.5*	5.4*	100	-
Ghafariyasl et al., 2012, [21]	N3, Elastix, BET	intensity and area threshold	FFFS → LDC, QDC, SVC, Parzen	90.9	-	-	4.1	1.8*	-	-
Kuijf et al., 2012, [33]	SPM8, normalization, standardization	3D RST	manual inspection	71.2	-	-	17.17	4.68*	-	-
Kuijf et al., 2013, [35]	SPM8, normalization, standardization	3D RST	manual inspection	87	-	-	45	-	-	-
Bian et al., 2013, [26]	BET, ARC, mIP, normalization	FRST	vessel mask screening, 3D region growing, geometric features	86.5	-	-	44.9	1.5*	-	-
Fazlollahi et al., 2013, [41]	CSF, inversion, normalization, Gaussian blur	multi-scale ID line detection	center detection → Hessian matrix	100	-	-	158.93*	-	99.9	-
Fazlollahi et al., 2014, [28]	N4, CSF, skull-stripping, normalization, equalization, anisotropic diffusion	multi-scale Laplacian of Gaussian	3D Rodon Transform → Hessian matrix, RFC	92.04	-	-	16.84	6.7*	-	-
Fazlollahi et al., 2015, [27]	N4, CSF, inversion, normalization, equalization, anisotropic	Laplacian of Gaussian	3D Rodon Transform → Hessian matrix, RFC	87	-	-	27.1	-	-	-

Roy et al., 2015, [44]	diffusion N4, skull stripping, phase enhancement	3D region growing	RST, WM mask, geometric features	85.7	-	-	-	-	99.5	-
Chen et al., 2015, [42]	normalization	intensity threshold	CNN, 3D concatenation, SVM	89.13	56.16	68.91	6.4	-	-	-
Dou et al., 2015, [43]	normalization	intensity threshold	ISA SVM	89.44	-	-	7.7	0.9	-	-
van den Heuvel et al., 2015, [45]	FSL FLIRT, FSL FAST, N3, SPM12b, normalization	voxel based features → RFC	-	90	-	-	-	1.3	-	-
Dou et al., 2016, [3]	slices merging	hierarchical 3D CNN	3D CNN	93.16	44.31	60.06	2.74	-	-	-
Zhang et al., 2016, [46]	reconstruction Syngo MR B17, SNP	SAE	-	93.20	-	-	-	-	93.25	93.22
van den Heuvel et al., 2016, [29]	FSL FLIRT, FSL FAST, N3, SPM12b	voxel based features → RFC	object classifier, growing-based algorithm	93	-	-	25.9	0.29	-	-
Lu et al., 2017, [22]	square window size	CNN	-	97.29	-	-	-	-	92.23	96.05
Wang et al., 2017, [53]	SNP, discard borders, cost ratio	CNN+RAP	-	96.94	-	-	-	-	97.18	97.18
Tajudin et al., 2017, [137]	-	watershed transform, active contour analysis (Chan-Vese)	-	Authors provided only mean square error MSE = 0.089 and peak signal to noise ratio PSNR = 34.5221						
Standvoss et al., 2018, [140]	augmentation, selective sampling	3D CNN, connected component analysis	-	87	-	-	16.75	2.5	-	-
Zhang et al., 2018, [47]	SNP, discard borders, cost ratio	ANN	-	93.05	-	-	-	-	93.06	93.06
Zhang et al.,	SNP,	SAE-DNN	-	95.13	-	-	-	-	93.33	94.23



2018, [48]	discard borders									
Ateeq et al., 2018, [24]	Brainsuite	intensity threshold, filtering, hole filling	SVM, QDA, ensemble classifier	93.7	-	-	56	5.3	-	-
Morrison et al., 2018, [51]	BET	FRST	region growing, geometric features, manual validation	86.7	-	-	44.9	1.5*	-	-
Bao et al., 2018, [52]	SNP	Bayesian classifier	-	74.53	-	-	-	-	74.51	74.52
Tao et al., 2018, [139]	SNP	GA-BPNN	-	72.90	-	-	-	-	72.89	72.90
Gunter et al., 2018, [78]	intensity threshold, image cut, data augmentation	CNN	-	Authors provided only AUC = 98.5						
Liu et al., 2019, [5]	N4, SWI generation, resize, normalization	3D FRST	3D CNN	95.80	70.90	81.49*	1.6	0.39	-	-
Chen et al., 2019, [17]	ARC, BET, SWI generation, negative phase mask	FRST	manual validation, 3D ResNet	94.69	71.98	81.79	11.58	-	-	-
<b>Wang et al., 2019, [4]</b>	sliding window	Dense-Net 201	-	<b>97.78</b>	<b>97.65</b>	-	-	-	<b>97.64</b>	<b>97.71</b>
Hong et al., 2019, [14]	SNP	ResNet50	-	95.71	-	-	-	-	99.21	97.46
Hong et al., 2019, [77]	SNP	CNN	-	98.87	-	-	-	-	96.49	97.68
Sa-ngiem et al., 2019, [126]	intensity enhancement, binarization, morphological operations, geometrical features	AlexNet, brain area extraction	-	-	-	-	-	-	-	95.45

Hong et al., 2020, [23]	SNP, brain area enhancement	CNN	-	99.74	-	-	-	96.89	98.32
Doke et al., 2020, [124]	sliding window, augmentation	CNN	-	98.97	99.66	-	-	98.14	98.54
Liu et al., 2020, [76]	binarization, noise reduction	Fourier descriptor	-	85.2	3.2	-	69.5	-	-
Lu et al., 2020, [125]	reconstruction Syngo MR B17, SNP	VGG-ELM-BAC	-	93.08	-	-	-	87.12	90.00
Al-masni et al., 2020, [30, 1]	BET, slices merging	YOLOv2	3D-CNN	94.32	61.94	74.78	1.42	-	-
Rashid et al., 2020, [6]	N4, QSM generation, padding, normalization, augmentation	U-Net	-	84	59	-	-	-	-
Chesebro et al., 2021, [2]	BET, CSF mask, resize	Sobel filter, Hough transform	CSF filtering, 3D geometric filtering, manual validation	95.00	11.00	19.72	9.7	-	-
Myung et al., 2021, [13]	BET augmentation	YOLO	CSF filtering	66.90	79.75	72.76	2.15	-	-
Li et al., 2021, [19]	ANTs, JPG conversion, augmentation	SSD + FE	-	90	79.7	84.54*	-	0.23	-
Ferlin et al., 2021, [18]	padding, resize, standardization, slices merging, annotations modification augmentation	Faster RCNN	overlap between slices	92.62	89.74	90.84	0.24	-	-
Lu et al., 2021, [49]	SNP	CNN+ELM+BA	-	92.93	-	-	-	83.35	88.56
Lu et al., 2021, [75]	SNP	CNN+EN	-	98.27	-	-	-	98.93	98.60
Momeni et al.,	N4,	ANN	-	18.6	9.2	-	3.6	99.4	96.8

2021, [74]	augmentation, synthetic CMBs generation BrainSuite, augmentation	K-means clustering, geometrical features	Alex-Net	97.26	-	-	-	96.5	96.21
<b>Stanley et al., 2022, [72]</b>	resize, contrast stretching, normalization, Gaussian Filter, histogram equalization, morphological operations, Sharr gradient, 3D GCM	1D CNN+LSTM	-	<b>98.76</b>	-	<b>98.78</b>	-	<b>97.21</b>	<b>98.24</b>
Sundersan et al., 2022, [20]	fsloreorient2std, FSL FAST, BET	Frangi filters, FRST, intensity transformations, eigenvalues, Gaussian filter, Laplacian of Gaussian	geometric features level threshold	91	-	-	-	81	86

<sup>1</sup>Data marked with \* were not provided in original paper. Instead, they were calculated either by us or the Authors of other papers listed in Table 3, based on data provided in the original paper.

### 3.5 Comparison of existing approaches

Table 3 presents, in chronological order, multiple approaches regarding cerebral microbleed detection that had place in recent years. It can be observed that firstly, the prevailing solutions were those based on traditional image processing techniques and only later the proposals based on machine learning algorithms have taken the lead. It can be seen, that they achieved considerably higher performance, both in terms of sensitivity and low false positive generation. Therefore, it can be assumed that this latter path is more promising regarding practically applicable solutions. Alternatively, a combination of traditional and ML methods might be considered.

Regarding the pre-processing stage, there are several operations, such as bias field correction, skull stripping and normalization, that should be done before providing data into the system. Other transforms may also be used in particular cases, but they are not essential.

An important issue is related with selecting the type of solved problem: whether it should be classification, detection, or segmentation. A large part of solutions is based on cutting images into smaller fragments and their further classification. These approaches are reported to have significantly better ability to distinguish CMB from its mimic. On the other hand, in the case of detection, a lot of false positive predictions are generated, which often forces introducing the second stage, namely false positive reduction or predictions verification, as high false positive generation is the main problem in CMBs detection. Another challenge that can be overcome by using classification instead of detection is the size of the lesion. CMBs are small objects, which makes them difficult to find in the original image.

No significant improvement can be seen for 3D CNN over 2D CNN. Probably, a larger training dataset could enable taking benefit from the 3D CNN structure and consequently achieve better results. For now, however, choosing this type of solution is discouraging, due to higher computation cost.

Moreover, it is clearly visible, that the reported research often lack in some metrics. Even if we accept that mentioning all of indicators is not necessary, it is crucial to provide a proper evaluation.

We would like to emphasize that in our opinion, based on the gathered data, it is difficult to state which approach is the best and it is still the area that requires development. However, we can draw attention to some most promising solutions: in case of classification [72, 4] and [75] with the best ACC=98.60%; while in case of detection [19] and [18] with F1=90.84%. The mentioned research distinguish also in terms of balanced results - similar values of all metrics, which is an advantage in comparison to for instance [1, 30, 2] that report higher sensitivity, however suffer from a high false positive predictions generation - low precision.

Although [124, 23] also report high accuracy, the datasets used by them were small. Results reported in [72, 18, 19] were performed on relatively big, but diverse datasets, therefore are hard to compare. From mentioned proposals only [4] and [75] can be compared, as they used the same, but small dataset.

Nevertheless, the above careful and comprehensive analysis provides an opportunity to formulate some conclusions, outline best practices, and point out the key elements of a reliable automatic cerebral microbleeds detection system.

## 4 Discussion

In this section we discuss the most important aspects for automatic CMBs detection system.

As previously mentioned, a base for any automatic system, especially machine learning model, is the data. Although traditional image processing methods do not require large amount of data for training, just for validation and testing purposes, it is still essential for proper system evaluation.

In Section 2 a range of datasets is listed which were used in all reported approaches. These datasets differ not only in terms of acquisition parameters, but also by the origin and medical history of patients. This kind of diversity makes any comparison of newly proposed approaches almost impossible. Moreover, some datasets have extremely small number of subjects [25, 32]. In that case, the tested subset is not representative enough. The system trained on such a narrowed dataset will reveal low generalization ability [29]. Therefore, a big, diversified dataset is needed and advanced regularization techniques should be applied [149] to prevent over-fitting.

An interesting approach to overcome the data shortage problem was proposed by Momeni et al. [74]. It consisted of synthetic microbleeds generation based on previously extracted CMB features. Another way to produce huge amounts of synthesized data are Generative Adversarial Networks (GANs) [141]. They are able to create new images based on the features automatically extracted from the existing, real dataset. However, again, it is a method that requires relatively large dataset at the beginning. Despite the risk of biased data generation, both approaches seem promising for extending datasets, next to other augmentation methods.

A good practice regarding a general system evaluation is using a completely unrelated dataset for testing to ensure that the obtained results are impartial like in [18, 74]. The term *unrelated dataset* means the data acquired from a different MRI machine, from subjects of different origin and medical history, and ranked by another rater. Examinations performed on various MRI machines may differ in parameters. It is important to synthesize system resistant to features that do not have a direct impact on prediction. Usage of various datasets ensures insight into the model's generalization ability. This, however, is an ideal situation, not always achievable in practice.

There are also methods such as k-fold validation that may enable better evaluation within the same dataset. It is recommended especially during system development as depending on chosen training, validation and testing sets, the obtained results may differ [1, 30, 18]. Another idea is preparation of a system nameplate with detailed description of system properties and target data type and it should point out operating conditions of the system and its limitations.

The unavailability of the used datasets is another limitation in terms of approach comparison. Although there are many legal restrictions regarding medical data sharing, establishing a benchmark dataset would significantly trigger the development in this domain [146], similarly as it was in case of brain glioma segmentation [156] or determining skeletal age [158, 157].

Another aspect is the pre-processing stage of system synthesis. Subjecting images to any transformations should be well-thought and justified. Considering the risk of valuable data loss, precautions should be taken to prevent that.

A common method of pre-processing is bias field correction as it enables restoring some important information. Using dedicated tools for skull stripping seems to be a better approach than simply removing part of the image just as in [47, 48, 53]. Although unintentionally, the image passed to the system may still be deformed or partial. Any operations that modify the size of the image, should be performed without content loss just as in [20].

When it comes to system designing, there are several issues that should be considered. Firstly, the MRI data is given in the three-dimensional space. Regardless the used algorithms, at some stage it is inevitable to use the information from the third dimension. Especially, when detecting cerebral microbleeds is concerned, that kind of data is very important, as it enables distinguishing the CMBs from their most common mimics - vessels [26, 28, 42, 3, 5, 17, 1, 2, 18]. While vessels can be distinguished based on 3D information, the other CMB mimic - calcification looks similar also in the 3D space considering its shape. In such case, other MRI sequences, except SWI, may be helpful [1].

In the majority of reported research, the solution process is divided into three stages: *Pre-processing*, *CMB Candidates Detection*, and *CMB Candidates Verification* (Table 3). This approach is caused by similarities between CMBs and their mimics, with consequent high production of false positive candidates. All this compels the use of *CMB Candidates verification* stage to eliminate FP candidates. It may extend the computation time, but it is necessary to obtain satisfying results. Still, keeping the balance between accuracy and efficiency is important, particularly when real-time usage is concerned.

The next, worth considering issue is the nature of cerebral microbleeds. They are small hemorrhages, which are sometimes difficult to notice even for an experienced radiologist. Therefore, the system to be designed should be sensitive to small objects. For this purpose, automatic systems may turn out even better, as they are able to consider the information that is not visible for human eye. It is also important to note that more accurate and sensitive MRI machines with properly adjusted parameters increase the chance for finding all microbleeds [34].

Another problem is related to the possibility of missing some CMBs by an experienced rater. In any research regarding detection a ground truth has to be established. However, this is extremely difficult, as the rater agreement may be at a relatively low level, for instance -  $\kappa = 0.68$  [73]. To reduce this problem, preliminary rating should be performed by as many raters as possible. Additionally, verification of system results may be helpful, as some missing CMBs may be detected by the system and should not be treated as false positive [74]. On the other hand, the radiologist has ability to look at the potential CMB from different perspectives and consult it with others, whereas the system does not. Therefore, providing additional information about gender, age, injury, angiography scans, etc. might also turn out beneficial [35].

When designing such a system from the clinical application point of view, certain practical aspects must also be taken into account. It is important to remember about the end-user's perspective. In this context, the form of results presentation should be designed considering user experience.

Obviously, the indication by a bounding-box or circle should be provided, but other useful information such as the confidence score of the prediction could also be included. This value is rather provided by the machine-learning system, but it gives the information to the radiologist about certainty, which can accelerate the rating process.

Other idea might be the presentation of results based on the existing rating scales such as MARS [69] or BOMBS [7] (Section 2.2).

Moreover, there should be the ability of result acceptance or rejection. As the system to be designed is the *computer aided* system, the user should have the possibility to agree with the proposed result or not, as his decision is final. This decision, however, has to be strongly distinguished from involving a human in the loop. The raters have knowledge essential for CMBs rating, therefore they may be used during system design, for instance to validate preliminary results or to label extracted candidates as CMB and non-CMB, similarly as in [17], but they should not be used as the last stage of the process to increase the system performance. The reported 100% precision or specificity of a semi-automated system in which a human is part of the FP reduction process is simply misleading [25, 35, 51]. Even if it significantly reduces the single scan rating time, this type of evaluation is confusing.

However, the feedback from the radiologist about the prediction may be used for continual learning [159]. This kind of approach may cause improvement of the already working system.

This smoothly leads to the problem of system evaluation. Section 3.4 presented different metrics and their correlations. Depending on the selected task: classification, detection, or segmentation - different metrics are used. However, it is crucial to present as many metrics as possible, as they focus on different aspects of the system. The sensitivity of 99% may seem an outstanding result, but when it goes with precision of 40% it is not satisfying. The researchers sometimes stress out the importance of sensitivity and diminish the number of potential false positives, but it can be harmful in terms of reliable system synthesis [25]. All this leads to the conclusion that a properly designed system should be balanced and optimized as a whole.

System evaluation is also important for enabling comparison between different approaches. It is clearly visible in Table 3 that the researchers not always provide all necessary metrics, which significantly hinders identifying the state-of-the-art.

Despite the current levels of metrics, there is a general issue of system trustworthiness. While the systems based on morphological operations and traditional image transformations are pretty easy to explain, the interpretability of black-box machine-learning systems is still a challenging task [142, 143, 144]. This problem is crucial, especially in such a life-impacting domain as medicine. The process of decision making should be clear to ensure that the conclusions are drawn based on the nature of the examined object and not on the bias. Therefore, there is an urgent need of bias reduction [145]. A list of guidelines regarding designing a responsible and trustworthy AI system is given in [136].

To the best of our knowledge, the paper collates all available research reports regarding automatic cerebral microbleeds detection. The challenges of this task and some flaws of existing proposals have been outlined. We believe that this paper will serve as a mine of knowledge and ideas for further research within this domain. We hope that it will stimulate better practices regarding exchanging knowledge between different research groups.

## References

- [1] Al-masni, M., Kim, W., Kim, E., Noh, Y. & Kim, D. Automated detection of cerebral microbleeds in MR images: A two-stage deep learning approach. *NeuroImage: Clinical*. **28** pp. 102464 (2020), DOI: 10.1016/j.nicl.2020.102464, ISSN: 2213-1582
- [2] Chesebro, A., Amarante, E., Lao, P., Meier, I., Mayeux, R. & Brickman, A. Automated detection of cerebral microbleeds on T2\*-weighted MRI. *Scientific Reports*. **11**, 1-13 (2021), DOI: 10.1038/s41598-021-83607-0, ISSN: 20452322
- [3] Dou, Q., Chen, H., Yu, L., Zhao, L., Qin, J., Wang, D., Mok, V., Shi, L. & Heng, P. Automatic Detection of Cerebral Microbleeds from MR Images via 3D Convolutional Neural Networks. *IEEE Transactions On Medical Imaging*. **35**, 1182-1195 (2016), DOI: 10.1109/TMI.2016.2528129, ISSN: 1558254X
- [4] Wang, S., Tang, C., Sun, J. & Zhang, Y. Cerebral micro-bleeding detection based on densely connected neural network. *Frontiers In Neuroscience*. **13**, 1-11 (2019), DOI: 10.3389/fnins.2019.00422, ISSN: 1662453X
- [5] Liu, S., Utraiainen, D., Chai, C., Chen, Y., Wang, L., Sethi, S., Xia, S. & Haacke, E. Cerebral microbleed detection using Susceptibility Weighted Imaging and deep learning. *NeuroImage*. **198**, 271-282 (2019), DOI: 10.1016/j.neuroimage.2019.05.046, ISSN: 10959572
- [6] Rashid, T., Abdulkadir, A., Nasrallah, I., Ware, J., Liu, H., Spincemaille, P., Romero, J., Bryan, R., Heckbert, S. & Habes, M. DEEPMIR: a deep neural network for differential detection of cerebral microbleeds and iron deposits in MRI. *Scientific Reports*. **11**, 14124 (2021), DOI: 10.1038/s41598-021-93427-x, ISSN: 2045-2322
- [7] Cordonnier, C., Potter, G., Jackson, C., Doubal, F., Keir, S., Sudlow, C., Wardlaw, J. & Al-Shahi Salman, R. Improving interrater agreement about brain microbleeds: Development of the Brain Observer MicroBleed Scale (BOMBS). *Stroke*. **40**, 94-99 (2009), DOI: 10.1161/STROKEAHA.108.526996, ISSN: 00392499

- [8] Mazurek, M., Papuc, E. & Rejdak, K. Czynniki wpływające na występowanie mikrokrwawień mózgowych. *Polski Przegląd Neurologiczny*. **14**, 151-155 (2018), ISSN: 1734-9745, in polish
- [9] Shams, S., Granberg, T., Martola, J., Li, X., Shams, M., Fereshtehnejad, S., Cavallin, L., Aspelin, P., Kristoffersen-Wiberg, M. & Wahlund, L. Cerebrospinal fluid profiles with increasing number of cerebral microbleeds in a continuum of cognitive impairment. *Journal Of Cerebral Blood Flow And Metabolism : Official Journal Of The International Society Of Cerebral Blood Flow And Metabolism*. **36**, 621-628 (2016), DOI: 10.1177/0271678X15606141, ISSN: 1559-7016 (Electronic)
- [10] Akoudad, S., Portegies, M., Koudstaal, P., Hofman, A., Lugt, A., Ikram, M. & Vernooij, M. Cerebral Microbleeds Are Associated With an Increased Risk of Stroke: The Rotterdam Study. *Circulation*. **132**, 509-516 (2015), DOI: 10.1161/CIRCULATIONAHA.115.016261, ISSN: 1524-4539 (Electronic)
- [11] Yakushiji, Y., Nishiyama, M., Yakushiji, S., Hirotsu, T., Uchino, A., Nakajima, J., Eriguchi, M., Nanri, Y., Hara, M., Horikawa, E. & Kuroda, Y. Brain microbleeds and global cognitive function in adults without neurological disorder. *Stroke*. **39**, 3323-3328 (2008), DOI: 10.1161/STROKEAHA.108.516112, ISSN: 00392499
- [12] Greenberg, S., Vernooij, M., Cordonnier, C., Viswanathan, A., Al-Shahi Salman, R., Warach, S., Launer, L., Van Buchem, M. & Breteler, M. Cerebral microbleeds: a guide to detection and interpretation. *The Lancet Neurology*. **8**, 165-174 (2009), DOI: 10.1016/S1474-4422(09)70013-4, ISSN: 14744422
- [13] Myung, M., Lee, K., Kim, H., Oh, J., Lee, J., Shin, I., Kim, E. & Lee, J. Novel Approaches to Detection of Cerebral Microbleeds: Single Deep Learning Model to Achieve a Balanced Performance. *Journal Of Stroke And Cerebrovascular Diseases*. **30**, 105886 (2021), DOI: 10.1016/j.jstrokecerebrovasdis.2021.105886, ISSN: 1052-3057
- [14] Hong, J., Cheng, H., Zhang, Y. & Liu, J. Detecting cerebral microbleeds with transfer learning. *Machine Vision And Applications*. **30**, 1123-1133 (2019), DOI: 10.1007/s00138-019-01029-5, ISSN: 14321769
- [15] He, K., Zhang, X., Ren, S. & Sun, J. Deep Residual Learning for Image Recognition. *2016 IEEE Conference On Computer Vision And Pattern Recognition (CVPR)*. pp. 770-778 (2016), DOI: 10.1109/CVPR.2016.90
- [16] Lupo, J., Banerjee, S., Hammond, K., Kelley, D., Xu, D., Chang, S., Vigneron, D., Majumdar, S. & Nelson, S. GRAPPA-based susceptibility-weighted imaging of normal volunteers and patients with brain tumor at 7 T. *Magnetic Resonance Imaging*. **27**, 480-488 (2009), DOI: 10.1016/j.mri.2008.08.003, ISSN: 0730-725X
- [17] Chen, Y., Villanueva-Meyer, J., Morrison, M. & Lupo, J. Toward Automatic Detection of Radiation-Induced Cerebral Microbleeds Using a 3D Deep Residual Network. *Journal Of Digital Imaging*. **32**, 766-772 (2019), DOI: 10.1007/s10278-018-0146-z, ISSN: 1618727X
- [18] Ferlin, M., Grochowski, M., Kwasigroch, A., Mikołajczyk, A., Szurowska, E., Grzywińska, M. & Sabisz, A. A Comprehensive Analysis of Deep Neural-Based Cerebral Microbleeds Detection System. *Electronics*. **10** (2021), DOI: 10.3390/electronics10182208, ISSN: 2079-9292
- [19] Li, T., Zou, Y., Bai, P., Li, S., Wang, H., Chen, X., Meng, Z., Kang, Z. & Zhou, G. Detecting cerebral microbleeds via deep learning with features enhancement by reusing ground truth. *Computer Methods And Programs In Biomedicine*. **204** (2021), DOI: 10.1016/j.cmpb.2021.106051, ISSN: 18727565
- [20] Sundaresan, V., Arthofer, C., Zamboni, G., Dineen, R., Rothwell, P., Sotiropoulos, S., Auer, D., Tozer, D., Markus, H., Miller, K., Dragonu, I., Sprigg, N., Alfaro-Almagro, F., Jenkinson, M. & Griffanti, L. Automated Detection of Candidate Subjects With Cerebral Microbleeds Using Machine Learning. *Frontiers In Neuroinformatics*. **15** pp. 777828 (2022), DOI: 10.3389/fninf.2021.777828, ISSN: 1662-5196
- [21] Ghafaryasl, B., Lijn, F., Poels, M., Vrooman, H., Ikram, M., Niessen, W., Lugt, A., Vernooij, M. & Bruijne, M. A computer aided detection system for cerebral microbleeds in brain MRI. *2012 9th IEEE International Symposium On Biomedical Imaging (ISBI)*. pp. 138-141 (2012), DOI: 10.1109/ISBI.2012.6235503
- [22] Lu, S., Lu, Z., Hou, X., Cheng, H. & Wang, S. Detection of cerebral microbleeding based on deep convolutional neural network. *2016 13th International Computer Conference On Wavelet Active Media Technology And Information Processing, ICCWAMTIP 2017. 2018-Febru* pp. 93-96 (2017), DOI: 10.1109/IC-CWAMTIP.2017.8301456, ISBN: 9781509061259
- [23] Hong, J., Wang, S., Cheng, H. & Liu, J. Classification of cerebral microbleeds based on fully-optimized convolutional neural network. *Multimedia Tools And Applications*. **79**, 15151-15169 (2020), DOI: 10.1007/s11042-018-6862-z, ISSN: 1380-7501, 1573-7721
- [24] Ateeq, T., Majeed, M., Anwar, S., Maqsood, M., Rehman, Z., Lee, J., Muhammad, K., Wang, S., Baik, S. & Mehmood, I. Ensemble-classifiers-assisted detection of cerebral microbleeds in brain MRI. *Computers & Electrical Engineering*. **69** pp. 768-781 (2018), DOI: 10.1016/j.compeleceng.2018.02.021, ISSN: 00457906

- [25] Barnes, S., Haacke, E., Ayaz, M., Boikov, A., Kirsch, W. & Kido, D. Semiautomated detection of cerebral microbleeds in magnetic resonance images. *Magnetic Resonance Imaging*. **29**, 844-852 (2011), <https://linkinghub.elsevier.com/retrieve/pii/S0730725X1100097X>, DOI: 10.1016/j.mri.2011.02.028, ISSN: 0730725X
- [26] Bian, W., Hess, C., Chang, S., Nelson, S. & Lupo, J. Computer-aided detection of radiation-induced cerebral microbleeds on susceptibility-weighted MR images. *NeuroImage: Clinical*. **2** pp. 282-290 (2013), DOI: 10.1016/j.nicl.2013.01.012, ISSN: 22131582
- [27] Fazlollahi, A., Meriaudeau, F., Giancardo, L., Villemagne, V., Rowe, C., Yates, P., Salvado, O. & Bourgeat, P. Computer-aided detection of cerebral microbleeds in susceptibility-weighted imaging. *Computerized Medical Imaging And Graphics*. **46** pp. 269-276 (2015), DOI: 10.1016/j.compmedimag.2015.10.001, ISSN: 08956111
- [28] Fazlollahi, A., Meriaudeau, F., Villemagne, V., Rowe, C., Yates, P., Salvado, O. & Bourgeat, P. Efficient machine learning framework for computer-aided detection of cerebral microbleeds using the Radon transform. *2014 IEEE 11th International Symposium On Biomedical Imaging (ISBI)*. pp. 113-116 (2014), DOI: 10.1109/ISBI.2014.6867822, ISBN: 978-1-4673-1961-4
- [29] Heuvel, T., Eerden, A., Manniesing, R., Ghafoorian, M., Tan, T., Andriessen, T., Vande Vyvere, T., Hauwe, L., Haar Romeny, B., Goraj, B. & Platel, B. Automated detection of cerebral microbleeds in patients with traumatic brain injury. *NeuroImage: Clinical*. **12** pp. 241-251 (2016), DOI: 10.1016/j.nicl.2016.07.002, ISSN: 22131582
- [30] Al-masni, M., Kim, W., Kim, E., Noh, Y. & Kim, D. A Two Cascaded Network Integrating Regional-based YOLO and 3D-CNN for Cerebral Microbleeds Detection. *2020 42nd Annual International Conference Of The IEEE Engineering In Medicine & Biology Society (EMBC)*. pp. 1055-1058 (2020), DOI: 10.1109/EMBC44109.2020.9176073, ISBN: 978-1-72811-990-8
- [31] Liu, T., Surapaneni, K., Lou, M., Cheng, L., Spincemaille, P. & Wang, Y. Cerebral Microbleeds: Burden Assessment by Using Quantitative Susceptibility Mapping. *Radiology*. **262**, 269-278 (2012), DOI: 10.1148/radiol.11110251, ISSN: 0033-8419, 1527-1315
- [32] Kuijf, H., Bresser, J., Biessels, G., Viergever, M. & Vincken, K. Detecting cerebral microbleeds in 7.0 T MR images using the radial symmetry transform. *2011 IEEE International Symposium On Biomedical Imaging: From Nano To Macro*. pp. 758-761 (2011), DOI: 10.1109/ISBI.2011.5872516, ISBN: 978-1-4244-4127-3
- [33] Kuijf, H., Bresser, J., Geerlings, M., Conijn, M., Viergever, M., Biessels, G. & Vincken, K. Efficient detection of cerebral microbleeds on 7.0T MR images using the radial symmetry transform. *NeuroImage*. **59**, 2266-2273 (2012), DOI: 10.1016/j.neuroimage.2011.09.061, ISSN: 10538119
- [34] Nandigam, R., Viswanathan, A., Delgado, P., Skehan, M., Smith, E., Rosand, J., Greenberg, S. & Dickerson, B. MR imaging detection of cerebral microbleeds: Effect of susceptibility-weighted imaging, section thickness, and field strength. *American Journal Of Neuroradiology*. **30**, 338-343 (2009), DOI: 10.3174/ajnr.A1355, ISSN: 01956108
- [35] Kuijf, H., Brundel, M., Bresser, J., Veluw, S., Heringa, S., Viergever, M., Biessels, G. & Vincken, K. Semi-Automated Detection of Cerebral Microbleeds on 3.0 T MR Images. *PLoS ONE*. **8**, e66610 (2013), DOI: 10.1371/journal.pone.0066610, ISSN: 1932-6203
- [36] Hofman, A., Breteler, M., Duijn, C., Krestin, G., Pols, H., Stricker, B., Tiemeier, H., Uitterlinden, A., Vingerling, J. & Witteman, J. The Rotterdam Study: objectives and design update. *European Journal Of Epidemiology*. **22**, 819-829 (2007), DOI: 10.1007/s10654-007-9199-x, ISSN: 0393-2990
- [37] Simons, P., Algra, A., Laak, M., Grobbee, D. & Graaf, Y. Second Manifestations of ARterial disease (SMART) study: Rationale and design. *European Journal Of Epidemiology*. **15**, 773-781 (1999), DOI: 10.1023/A:1007621514757, ISSN: 1573-7284
- [38] Heckbert, S., Austin, T., Jensen, P., Floyd, J., Psaty, B., Soliman, E. & Kronmal, R. Yield and consistency of arrhythmia detection with patch electrocardiographic monitoring: The Multi-Ethnic Study of Atherosclerosis. *Journal Of Electrocardiology*. **51**, 997-1002 (2018), DOI: 10.1016/j.jelectrocard.2018.07.027, ISSN: 1532-8430
- [39] Akiyama, Y., Miyata, K., Harada, K., Minamida, Y., Nonaka, T., Koyanagi, I., Asai, Y. & Houkin, K. Susceptibility-Weighted Magnetic Resonance Imaging for the Detection of Cerebral Microhemorrhage in Patients With Traumatic Brain Injury. *Neurologia Medico-chirurgica*. **49**, 97-99 (2009), DOI: 10.2176/nmc.49.97, ISSN: 0470-8105, 1349-8029
- [40] Park, J., Park, S., Kang, S., Nam, T., Min, B. & Hwang, S. Detection of Traumatic Cerebral Microbleeds by Susceptibility-Weighted Image of MRI. *Journal Of Korean Neurosurgical Society*. **46**, 365 (2009), DOI: 10.3340/jkns.2009.46.4.365, ISSN: 2005-3711



- [41] Fazlollahi, A., Meriaudeau, F., Villemagne, V., Rowe, C., Desmond, P., Yates, P., Salvado, O. & Bourgeat, P. Automatic detection of small spherical lesions using multiscale approach in 3D medical images. *2013 IEEE International Conference On Image Processing*. pp. 1158-1162 (2013), DOI: 10.1109/ICIP.2013.6738239, ISBN: 978-1-4799-2341-0
- [42] Chen, H., Yu, L., Dou, Q., Shi, L., Mok, V. & Heng, P. Automatic detection of cerebral microbleeds via deep learning based 3D feature representation. *2015 IEEE 12th International Symposium On Biomedical Imaging (ISBI)*. pp. 764-767 (2015), DOI: 10.1109/ISBI.2015.7163984, ISBN: 978-1-4799-2374-8
- [43] Qi Dou, Hao Chen, Lequan Yu, Lin Shi, Defeng Wang, Mok, V. & Pheng Ann Heng Automatic cerebral microbleeds detection from MR images via Independent Subspace Analysis based hierarchical features. *2015 37th Annual International Conference Of The IEEE Engineering In Medicine And Biology Society (EMBC)*. pp. 7933-7936 (2015), DOI: 10.1109/EMBC.2015.7320232, ISBN: 978-1-4244-9271-8
- [44] Roy, S., Jog, A., Magrath, E., Butman, J. & Pham, D. Cerebral microbleed segmentation from susceptibility weighted images. *Medical Imaging 2015: Image Processing*. **9413** pp. 364 - 370 (2015), DOI: 10.1117/12.2082237
- [45] T. L. A. van den Heuvel, M. Ghafoorian, A. W. van der Eerden M.D., B. M. Goraj, T. M. J. C. Andriessen, B. M. ter Haar Romeny & B. Platel Computer aided detection of brain micro-bleeds in traumatic brain injury. *Medical Imaging 2015: Computer-Aided Diagnosis*. **9414** pp. 94142F (2015), DOI: 10.1117/12.2075353
- [46] Zhang, Y., Hou, X., Lv, Y., Chen, H., Zhang, Y. & Wang, S. Sparse Autoencoder Based Deep Neural Network for Voxelwise Detection of Cerebral Microbleed. *2016 IEEE 22nd International Conference On Parallel And Distributed Systems (ICPADS)*. pp. 1229-1232 (2016), DOI: 10.1109/ICPADS.2016.0166, ISBN: 978-1-5090-4457-3
- [47] Zhang, Y., Hou, X., Chen, Y., Chen, H., Yang, M., Yang, J. & Wang, S. Voxelwise detection of cerebral microbleed in CADASIL patients by leaky rectified linear unit and early stopping. *Multimedia Tools And Applications*. **77**, 21825-21845 (2018), DOI: 10.1007/s11042-017-4383-9, ISSN: 1380-7501, 1573-7721
- [48] Zhang, Y., Zhang, Y., Hou, X., Chen, H. & Wang, S. Seven-layer deep neural network based on sparse autoencoder for voxelwise detection of cerebral microbleed. *Multimedia Tools And Applications*. **77**, 10521-10538 (2018), DOI: 10.1007/s11042-017-4554-8, ISSN: 1380-7501, 1573-7721
- [49] Lu, S., Liu, S., Wang, S. & Zhang, Y. Cerebral Microbleed Detection via Convolutional Neural Network and Extreme Learning Machine. *Frontiers In Computational Neuroscience*. **15** pp. 738885 (2021), DOI: 10.3389/fn-com.2021.738885, ISSN: 1662-5188
- [50] Wang, S., Sun, J., Mehmood, I., Pan, C., Chen, Y. & Zhang, Y. Cerebral micro-bleeding identification based on a nine-layer convolutional neural network with stochastic pooling. *Concurrency And Computation: Practice And Experience*. **32** (2020), DOI: 10.1002/cpe.5130, ISSN: 1532-0626, 1532-0634
- [51] Morrison, M., Payabvash, S., Chen, Y., Avadiappan, S., Shah, M., Zou, X., Hess, C. & Lupo, J. A user-guided tool for semi-automated cerebral microbleed detection and volume segmentation\_ Evaluating vascular injury and data labelling for machine learning. *Neuroimage: Clinical*. pp. 8 (2018), DOI: 10.1016/j.nicl.2018.08.002
- [52] Bao, F., Shi, M. & Macdonald, F. Voxelwise Detection of Cerebral Microbleed in CADASIL Patients by Naive Bayesian Classifier. *Proceedings Of The 2018 International Conference On Information Technology And Management Engineering (ICITME 2018)*. (2018), DOI: 10.2991/icitme-18.2018.35, ISBN: 978-94-6252-607-5
- [53] Wang, S., Jiang, Y., Hou, X., Cheng, H. & Du, S. Cerebral Micro-Bleed Detection Based on the Convolution Neural Network With Rank Based Average Pooling. *IEEE Access*. **5** pp. 16576-16583 (2017), DOI: 10.1109/ACCESS.2017.2736558, ISSN: 2169-3536
- [54] Loy, G. & Zelinsky, A. Fast radial symmetry for detecting points of interest. *IEEE Transactions On Pattern Analysis And Machine Intelligence*. **25**, 959-973 (2003), DOI: 10.1109/TPAMI.2003.1217601, ISSN: 0162-8828
- [55] Ashburner, J. & Friston, K. Unified segmentation. *NeuroImage*. **26**, 839-851 (2005), DOI: 10.1016/j.neuroimage.2005.02.018, ISSN: 10538119
- [56] Smith, S. Fast robust automated brain extraction. *Human Brain Mapping*. **17**, 143-155 (2002), DOI: 10.1002/hbm.10062, ISSN: 1065-9471, 1097-0193
- [57] Shattuck, D. & Leahy, R. BrainSuite: An automated cortical surface identification tool. *Medical Image Analysis*. pp. 14 (2002)
- [58] Chang, C. & Lin, C. LIBSVM: A library for support vector machines. *ACM Transactions On Intelligent Systems And Technology*. **2**, 1-27 (2011), DOI: 10.1145/1961189.1961199, ISSN: 2157-6904, 2157-6912

- [59] Tustison, N., Avants, B., Cook, P., Yuanjie Zheng, Egan, A., Yushkevich, P. & Gee, J. N4ITK: Improved N3 Bias Correction. *IEEE Transactions On Medical Imaging*. **29**, 1310-1320 (2010), DOI: 10.1109/TMI.2010.2046908, ISSN: 0278-0062, 1558-254X
- [60] Sled, J., Zijdenbos, A. & Evans, A. A nonparametric method for automatic correction of intensity nonuniformity in MRI data. *IEEE Transactions On Medical Imaging*. **17**, 87-97 (1998), DOI: 10.1109/42.668698, ISSN: 02780062
- [61] Klein, S., Staring, M., Murphy, K., Viergever, M. & Pluim, J. elastix: A Toolbox for Intensity-Based Medical Image Registration. *IEEE Transactions On Medical Imaging*. **29**, 196-205 (2010), DOI: 10.1109/TMI.2009.2035616, ISSN: 0278-0062, 1558-254X
- [62] Liu, W., Anguelov, D., Erhan, D., Szegedy, C., Reed, S., Fu, C. & Berg, A. SSD: Single Shot MultiBox Detector. *Computer Vision – ECCV 2016*. **9905** pp. 21-37 (2016), DOI: 10.1007/978-3-319-46448-0\_2, ISBN: 978-3-319-46447-3 978-3-319-46448-0
- [63] Ronneberger, O., Fischer, P. & Brox, T. U-Net: Convolutional Networks for Biomedical Image Segmentation. *ArXiv*. (2015), arXiv: 1505.04597
- [64] Liu, J., Liu, T., Rochefort, L., Ledoux, J., Khalidov, I., Chen, W., Tsiouris, A., Wisnieff, C., Spincemaille, P., Prince, M. & Wang, Y. Morphology enabled dipole inversion for quantitative susceptibility mapping using structural consistency between the magnitude image and the susceptibility map. *NeuroImage*. **59**, 2560-2568 (2012), DOI: 10.1016/j.neuroimage.2011.08.082, ISSN: 10538119
- [65] Zhang, Y., Brady, M. & Smith, S. Segmentation of brain MR images through a hidden Markov random field model and the expectation-maximization algorithm. *IEEE Transactions On Medical Imaging*. **20**, 45-57 (2001), DOI: 10.1109/42.906424, ISSN: 02780062
- [66] Jenkinson, M. & Smith, S. A global optimisation method for robust affine registration of brain images. *Medical Image Analysis*. **5**, 143-156 (2001), DOI: 10.1016/S1361-8415(01)00036-6, ISSN: 13618415
- [67] Jenkinson, M., Bannister, P., Brady, M. & Smith, S. Improved Optimization for the Robust and Accurate Linear Registration and Motion Correction of Brain Images. *NeuroImage*. **17**, 825-841 (2002), DOI: 10.1006/nimg.2002.1132, ISSN: 10538119
- [68] Breiman, L. Random Forests. *Machine Learning*. **45**, 5-32 (2001), DOI: 10.1023/A:1010933404324, ISSN: 1573-0565
- [69] Gregoire, S., Chaudhary, U., Brown, M., Yousry, T., Kallis, C., Jäger, H. & Werring, D. The Microbleed Anatomical Rating Scale (MARS). *Neurology*. **73**, 1759 (2009), DOI: 10.1212/WNL.0b013e3181c34a7d
- [70] Bian, W., Morrison, M., Zhu, X., Avadiappan, S., Chen, Y., Payabvash, S., Shah, M., Hess, C. & Lupo, J. CMB labeler. *Github*. (2018)
- [71] Real, R. & Vargas, J. The Probabilistic Basis of Jaccard's Index of Similarity. *SYSTEMATIC BIOLOGY*. **45** pp. 6 (1996)
- [72] Stanley, B. & Wilfred Franklin, S. Automated cerebral microbleed detection using selective 3D gradient co-occurrence matrix and convolutional neural network. *Biomedical Signal Processing And Control*. **75** pp. 103560 (2022), DOI: 10.1016/j.bspc.2022.103560, ISSN: 1746-8094
- [73] Seghier, M., Kolanko, M., Leff, A., Jäger, H., Gregoire, S. & Werring, D. Microbleed Detection Using Automated Segmentation (MIDAS): A New Method Applicable to Standard Clinical MR Images. *PLoS ONE*. **6**, e17547 (2011), DOI: 10.1371/journal.pone.0017547, ISSN: 1932-6203
- [74] Momeni, S., Fazlollahi, A., Yates, P., Rowe, C., Gao, Y., Liew, A. & Salvado, O. Synthetic microbleeds generation for classifier training without ground truth. *Computer Methods And Programs In Biomedicine*. **207** pp. 106127 (2021), DOI: 10.1016/j.cmpb.2021.106127, ISSN: 0169-2607
- [75] Lu, S., Nayak, D., Wang, S. & Zhang, Y. A cerebral microbleed diagnosis method via FeatureNet and ensembled randomized neural networks. *Applied Soft Computing*. **109** pp. 107567 (2021), DOI: 10.1016/j.asoc.2021.107567, ISSN: 1568-4946
- [76] Liu, H., Rashid, T. & Habes, M. Cerebral Microbleed Detection Via Fourier Descriptor with Dual Domain Distribution Modeling. *2020 IEEE 17th International Symposium On Biomedical Imaging Workshops (ISBI Workshops)*. pp. 1-4 (2020), DOI: 10.1109/ISBIWorkshops50223.2020.9153365
- [77] Hong, J., Cheng, H., Wang, S. & Liu, J. Improvement of Cerebral Microbleeds Detection Based on Discriminative Feature Learning. *Fundamenta Informaticae*. **168**, 231-248 (2019), DOI: 10.3233/FI-2019-1830, ISSN: 1875-8681

- [78] Gunter, J., Spsychalla, A., Ward, C., Graff-Radford, J., Huston, J., Kantarci, K., Knopman, D., Petersen, R. & Jack Jr., C. P4-232: Automating Cerebral Microbleed Detection in Support of Alzheimer's Disease Trials Using a Convolutional Neural Network Ai. *Alzheimer's & Dementia*. **14**, P1530-P1531 (2018), DOI: 10.1016/j.jalz.2018.07.053, ISSN: 1552-5279
- [79] Dou, Q., Chen, H., Qin, J. & Heng, P. CHAPTER NINE - Automatic lesion detection with three-dimensional convolutional neural networks. *Biomedical Information Technology (Second Edition)*. pp. 265-293 (2020), DOI: 10.1016/B978-0-12-816034-3.00009-2, ISBN: 978-0-12-816034-3
- [80] Chen, H., Dou, Q., Yu, L., Qin, J., Zhao, L., Mok, V., Wang, D., Shi, L. & Heng, P. Chapter 6 - Deep Cascaded Networks for Sparsely Distributed Object Detection from Medical Images. *Deep Learning For Medical Image Analysis*. pp. 133-154 (2017), DOI: 10.1016/B978-0-12-810408-8.00008-0, ISBN: 978-0-12-810408-8
- [81] Kirsch, W., McAuley, G., Holshouser, B., Petersen, F., Ayaz, M., Vinters, H., Dickson, C., Haacke, E., Britt III, W., Larsen, J., Kim, I., Mueller, C., Schrag, M. & Kido, D. Serial Susceptibility Weighted MRI Measures Brain Iron and Microbleeds in Dementia. *Journal Of Alzheimer's Disease*. **17**, 599-609 (2009), DOI: 10.3233/JAD-2009-1073, ISSN: 1387-2877
- [82] Mayeux, R. Washington Heights-Hamilton Heights-Inwood Columbia Aging Project. (Columbia University Irving Medical Center Neurological Institute, The Taub Institute for Research on Alzheimer's Disease), <https://cheba.unsw.edu.au/consortia/cosmic/studies/washington-heights-inwood-and-columbia-aging-project-whicap>, Accessed: 2022-06-01
- [83] Ellis, K., Bush, A., Darby, D., Fazio, D., Foster, J., Hudson, P., Lautenschlager, N., Lenzo, N., Martins, R., Maruff, P., Masters, C., Milner, A., Pike, K., Rowe, C., Savage, G., Szoeki, C., Taddei, K., Villemagne, V., Woodward, M., Ames, D. & Group, T. The Australian Imaging, Biomarkers and Lifestyle (AIBL) study of aging: methodology and baseline characteristics of 1112 individuals recruited for a longitudinal study of Alzheimer's disease. *International Psychogeriatrics*. **21**, 672-687 (2009), DOI: 10.1017/S1041610209009405, ISSN: 1741-203X, 1041-6102
- [84] Medical Education, M. & Research Alzheimer's Disease Research Center - Data Sharing and Resources. (<https://www.mayo.edu/research/centers-programs/alzheimers-disease-research-center/research-activities/mayo-clinic-study-aging/for-researchers/data-sharing-resources>), Accessed: 2022-04-04
- [85] Initiative, A. ADNI ACCESS DATA. (<https://adni.loni.usc.edu/data-samples/access-data/>), Accessed: 2022-04-04
- [86] Pacurar, E., Sethi, S., Habib, C., Laze, M., Martis-Laze, R. & Haacke, E. Database integration of protocol-specific neurological imaging datasets. *NeuroImage*. **124** pp. 1220-1224 (2016), DOI: 10.1016/j.neuroimage.2015.04.066, ISSN: 1053-8119
- [87] O'Donnell, H., Rosand, J., Knudsen, K., Furie, K., Segal, A., Chiu, R., Ikeda, D. & Greenberg, S. Apolipoprotein E Genotype and the Risk of Recurrent Lobar Intracerebral Hemorrhage. *New England Journal Of Medicine*. **342**, 240-245 (2000), DOI: 10.1056/NEJM200001273420403, ISSN: 0028-4793
- [88] Chen, Y., Gurol, M., Rosand, J., Viswanathan, A., Rakich, S., Groover, T., B.Eng., Greenberg, S. & Smith, E. Progression of white matter lesions and hemorrhages in cerebral amyloid angiopathy. *Neurology*. **67**, 83-87 (2006), DOI: 10.1212/01.wnl.0000223613.57229.24, ISSN: 0028-3878
- [89] Rothwell, P., Coull, A., Giles, M., Howard, S., Silver, L., Bull, L., Gutnikov, S., Edwards, P., Mant, D., Sackley, C., Farmer, A., Sandercock, P., Dennis, M., Warlow, C., Bamford, J. & Anslow, P. Change in stroke incidence, mortality, case-fatality, severity, and risk factors in Oxfordshire, UK from 1981 to 2004 (Oxford Vascular Study). *The Lancet*. **363**, 1925-1933 (2004), DOI: 10.1016/S0140-6736(04)16405-2, ISSN: 0140-6736
- [90] Sprigg, N., Flaherty, K., Appleton, J., Salman, R., Bereczki, D., Beridze, M., Christensen, H., Ciccone, A., Collins, R., Czlonkowska, A., Dineen, R., Duley, L., Egea-Guerrero, J., England, T., Krishnan, K., Laska, A., Law, Z., Ozturk, S., Pocock, S., Roberts, I., Robinson, T., Roffe, C., Seiffge, D., Scutt, P., Thanabalan, J., Werring, D., Whyne, D. & Bath, P. Tranexamic acid for hyperacute primary IntraCerebral Haemorrhage (TICH-2): an international randomised, placebo-controlled, phase 3 superiority trial. *The Lancet*. **391**, 2107-2115 (2018), DOI: 10.1016/S0140-6736(18)31033-X, ISSN: 0140-6736
- [91] Dineen, R., Pszczolkowski, S., Flaherty, K., Law, Z., Morgan, P., Roberts, I., Werring, D., Salman, R., England, T., Bath, P. & Sprigg, N. Does tranexamic acid lead to changes in MRI measures of brain tissue health in patients with spontaneous intracerebral haemorrhage? Protocol for a MRI substudy nested within the double-blind randomised controlled TICH-2 trial. *BMJ Open*. **8**, e019930 (2018), DOI: 10.1136/bmjopen-2017-019930
- [92] Centre, U. UK Biobank - UK Biobank. (<https://www.ukbiobank.ac.uk/>), Accessed: 2022-04-04

- [93] Song, S., Zheng, Y. & He, Y. A review of Methods for Bias Correction in Medical Images. *Biomedical Engineering Review*. **3** (2017), DOI: 10.18103/bme.v3i1.1550, ISSN: 23759143, 23759151
- [94] Patterson, D. Neuroimaging Core Documentation. (<https://neuroimaging-core-docs.readthedocs.io/en/latest/index.html>), Accessed: 2022-04-04
- [95] Human Neuroimaging, U. SPM. (<https://www.fil.ion.ucl.ac.uk/spm/>), Accessed: 2022-04-04
- [96] Penny, W., Friston, K., Ashburner, J., Kiebel, S. & Nicholas, T. Statistical Parametric Mapping: The Analysis of Functional. (Academic Press,2006), ISBN: 978-0-12-372560-8
- [97] Carass, A., Wheeler, M., Cuzzocreo, J., Bazin, P., Bassett, S. & Prince, J. A joint registration and segmentation approach to skull stripping. *2007 4th IEEE International Symposium On Biomedical Imaging*. pp. 656-659 (2007), DOI: 10.1109/ISBI.2007.356937, ISBN: 1424406722
- [98] Carass, A., Cuzzocreo, J., Wheeler, M., Bazin, P., Resnick, S. & Prince, J. Simple paradigm for extra-cerebral tissue removal: Algorithm and analysis. *NeuroImage*. **56**, 1982-1992 (2011), DOI: 10.1016/j.neuroimage.2011.03.045, ISSN: 10538119
- [99] Seghier, M., Ramlackhansingh, A., Crinion, J., Leff, A. & Price, C. Lesion identification using unified segmentation-normalisation models and fuzzy clustering. *NeuroImage*. **41**, 1253-1266 (2008), DOI: 10.1016/j.neuroimage.2008.03.028, ISSN: 10538119
- [100] Soille, P. Morphological Image Analysis. (Springer Berlin Heidelberg,2004), DOI: 10.1007/978-3-662-05088-0, ISBN: 978-3-642-07696-1 978-3-662-05088-0
- [101] Buslaev, A., Iglovikov, V., Khvedchenya, E., Parinov, A., Druzhinin, M. & Kalinin, A. Alumentations: Fast and Flexible Image Augmentations. *Information*. **11** (2020), DOI: 10.3390/info11020125, ISSN: 2078-2489
- [102] Paszke, A., Gross, S., Massa, F., Lerer, A., Bradbury, J., Chanan, G., Killeen, T., Lin, Z., Gimelshein, N., Antiga, L., Desmaison, A., Kopf, A., Yang, E., DeVito, Z., Raison, M., Tejani, A., Chilamkurthy, S., Steiner, B., Fang, L., Bai, J. & Chintala, S. PyTorch: An Imperative Style, High-Performance Deep Learning Library. *Advances In Neural Information Processing Systems 32*. pp. 8024-8035 (2019)
- [103] Li, N., Wang, W., Sati, P., Pham, D. & Butman, J. Quantitative assessment of susceptibility-weighted imaging processing methods. *Journal Of Magnetic Resonance Imaging : JMRI*. **40**, 1463-1473 (2014), DOI: 10.1002/jmri.24501, ISSN: 1522-2586
- [104] Tsushima, Y., Tanizaki, Y., Aoki, J. & Endo, K. MR Detection of microhemorrhages in neurologically healthy adults. *Neuroradiology*. **44**, 31-36 (2002), DOI: 10.1007/s002340100649, ISSN: 0028-3940, 1432-1920
- [105] Kaaouana, T., Bertrand, A., Ouamer, F., Law-ye, B., Pyatigorskaya, N., Bouyahia, A., Thiery, N., Dufouil, C., Delmaire, C., Dormont, D., Rochefort, L. & Chupin, M. Improved cerebral microbleeds detection using their magnetic signature on T2\*-phase-contrast: A comparison study in a clinical setting. *NeuroImage: Clinical*. **15** pp. 274-283 (2017), DOI: 10.1016/j.nicl.2016.08.005, ISSN: 22131582
- [106] Cordonnier, C., Al-Shahi Salman, R. & Wardlaw, J. Spontaneous brain microbleeds: systematic review, subgroup analyses and standards for study design and reporting. *Brain*. **130**, 1988-2003 (2007), DOI: 10.1093/brain/awl387, ISSN: 0006-8950, 1460-2156
- [107] Charidimou, A. & Werring, D. Cerebral microbleeds: detection, mechanisms and clinical challenges. *Future Neurology*. **6**, 587-611 (2011), DOI: 10.2217/fnl.11.42, ISSN: 1479-6708, 1748-6971
- [108] Charidimou, A., Krishnan, A., Werring, D. & Rolf Jäger, H. Cerebral microbleeds: a guide to detection and clinical relevance in different disease settings. *Neuroradiology*. **55**, 655-674 (2013), DOI: 10.1007/s00234-013-1175-4, ISSN: 0028-3940, 1432-1920
- [109] Charidimou, A., Jäger, H. & Werring, D. Cerebral microbleed detection and mapping: Principles, methodological aspects and rationale in vascular dementia. *Experimental Gerontology*. **47**, 843-852 (2012), DOI: 10.1016/j.exger.2012.06.008, ISSN: 05315565
- [110] Filippi, M., Horsfield, M., Bressi, S., Martinelli, V., Baratti, C., Reganati, P., Campi, A., Miller, D. & Comi, G. Intra- and inter-observer agreement of brain MRI lesion volume measurements in multiple sclerosis: A comparison of techniques. *Brain*. **118**, 1593-1600 (1995), DOI: 10.1093/brain/118.6.1593, ISSN: 0006-8950
- [111] Cheng, A., Batool, S., McCreary, C., Lauzon, M., Frayne, R., Goyal, M. & Smith, E. Susceptibility-Weighted Imaging is More Reliable Than T2\*-Weighted Gradient-Recalled Echo MRI for Detecting Microbleeds. *Stroke*. **44**, 2782-2786 (2013), DOI: 10.1161/STROKEAHA.113.002267, ISSN: 0039-2499, 1524-4628
- [112] Vernooij, M., Ikram, M., Wielopolski, P., Krestin, G., Breteler, M. & Lugt, A. Cerebral Microbleeds: Accelerated 3D T2\*-weighted GRE MR Imaging versus Conventional 2D T2\*-weighted GRE MR Imaging for Detection. *Radiology*. **248**, 272-277 (2008), DOI: 10.1148/radiol.2481071158, ISSN: 0033-8419

- [113] Shams, S., Martola, J., Cavallin, L., Granberg, T., Shams, M., Aspelin, P., Wahlund, L. & Kristoffersen-Wiberg, M. SWI or T2\*: Which MRI Sequence to Use in the Detection of Cerebral Microbleeds? The Karolinska Imaging Dementia Study. *American Journal Of Neuroradiology*. **36**, 1089-1095 (2015), DOI: 10.3174/ajnr.A4248, ISSN 0195-6108, 1936-959X
- [114] Scheid, R., Ott, D., Roth, H., Schroeter, M. & Cramon, D. Comparative Magnetic Resonance Imaging at 1.5 and 3 Tesla for the Evaluation of Traumatic Microbleeds. *Journal Of Neurotrauma*. **24**, 1811-1816 (2007), DOI: 10.1089/neu.2007.0382, ISSN: 0897-7151
- [115] Conijn, M., Geerlings, M., Biessels, G., Takahara, T., Witkamp, T., Zwanenburg, J., Luijten, P. & Hendrikse, J. Cerebral Microbleeds on MR Imaging: Comparison between 1.5 and 7T. *American Journal Of Neuroradiology*. **32**, 1043-1049 (2011), DOI: 10.3174/ajnr.A2450, ISSN: 0195-6108, 1936-959X
- [116] Bresser, J., Brundel, M., Conijn, M., Dillen, J., Geerlings, M., Viergever, M., Luijten, P. & Biessels, G. Visual Cerebral Microbleed Detection on 7T MR Imaging: Reliability and Effects of Image Processing. *American Journal Of Neuroradiology*. **34**, E61-E64 (2013), DOI: 10.3174/ajnr.A2960, ISSN: 0195-6108, 1936-959X
- [117] Liu, S., Buch, S., Chen, Y., Choi, H., Dai, Y., Habib, C., Hu, J., Jung, J., Luo, Y., Utriainen, D., Wang, M., Wu, D., Xia, S. & Haacke, E. Susceptibility Weighted Imaging: Current Status and Future Directions. *NMR In Biomedicine*. **30**, 10.1002/nbm.3552 (2017), DOI: 10.1002/nbm.3552, ISSN: 0952-3480
- [118] Reserve, C. MRI Basics. (<https://case.edu/med/neurology/NR/MRI>)
- [119] Werring, D. Cerebral Microbleeds: Clinical and Pathophysiological Significance. *Journal Of Neuroimaging*. **17**, 193-203 (2007), DOI: 10.1111/j.1552-6569.2006.00070.x, ISSN: 10512284, 15526569
- [120] Shoamanesh, A., Kwok, C. & Benavente, O. Cerebral Microbleeds: Histopathological Correlation of Neuroimaging. *Cerebrovascular Diseases*. **32**, 528-534 (2011), DOI: 10.1159/000331466, ISSN: 1421-9786, 1015-9770
- [121] Martinez-Ramirez, S., Greenberg, S. & Viswanathan, A. Cerebral microbleeds: overview and implications in cognitive impairment. *Alzheimer's Research & Therapy*. **6**, 33 (2014), DOI: 10.1186/alzrt263, ISSN: 1758-9193
- [122] Imaios Introduction to MRI sequences. (<https://www.imaios.com/en/e-Courses/e-MRI/MRI-Sequences/MRI-sequences>), ISBN 978-1847537768, Accessed: 2022-04-29
- [123] Lipton, M. Image Contrast: T1, T2, T2, and Proton Density. *Totally Accessible MRI: A User's Guide To Principles, Technology, And Applications*. pp. 38-46 (2008), DOI: 10.1007/978-0-387-48896-7\_4, ISBN: 978-0-387-48896-7
- [124] Doke, P., Shrivastava, D., Pan, C., Zhou, Q. & Zhang, Y. Using CNN with Bayesian optimization to identify cerebral micro-bleeds. *Machine Vision And Applications*. **31**, 36 (2020), DOI: 10.1007/s00138-020-01087-0, ISSN: 0932-8092, 1432-1769
- [125] Lu, S., Xia, K. & Wang, S. Diagnosis of cerebral microbleed via VGG and extreme learning machine trained by Gaussian map bat algorithm. *Journal Of Ambient Intelligence And Humanized Computing*. (2020), DOI: 10.1007/s12652-020-01789-3, ISSN: 1868-5137, 1868-5145
- [126] Sa-ngiem, S., Dittakan, K., Temkiatvises, K., Yaisoongnern, S. & Kespechara, K. Cerebral Microbleed Detection by Extracting Area and Number from Susceptibility Weighted Imagery Using Convolutional Neural Network. *Journal Of Physics: Conference Series*. **1229**, 012038 (2019), DOI: 10.1088/1742-6596/1229/1/012038, ISSN: 1742-6588, 1742-6596
- [127] Jenkinson, M., Beckmann, C., Behrens, T., Woolrich, M. & Smith, S. FSL. *Neuroimage*. **62**, 782-790 (2012), DOI: 10.1016/j.neuroimage.2011.09.015
- [128] Huang, G., Zhu, Q. & Siew, C. Extreme learning machine: Theory and applications. *Neurocomputing*. **70**, 489-501 (2006), DOI: 10.1016/j.neucom.2005.12.126, ISSN: 09252312
- [129] Ren, S., He, K., Girshick, R. & Sun, J. Faster R-CNN: Towards Real-Time Object Detection with Region Proposal Networks. *Proceedings Of The 28th International Conference On Neural Information Processing Systems - Volume 1*. pp. 91-99 (2015)
- [130] Redmon, J. & Farhadi, A. YOLO9000: Better, Faster, Stronger. *Proceedings Of The IEEE Conference On Computer Vision And Pattern Recognition (CVPR)*. (2017)
- [131] Krizhevsky, A., Sutskever, I. & Hinton, G. ImageNet Classification with Deep Convolutional Neural Networks. *Advances In Neural Information Processing Systems*. **25** (2012)
- [132] Simonyan, K. & Zisserman, A. Very Deep Convolutional Networks for Large-Scale Image Recognition. (2015), arXiv:1409.1556

- [133] Huang, G., Liu, Z., Maaten, L. & Weinberger, K. Densely Connected Convolutional Networks. (2018), arXiv:1608.06993
- [134] Barnard, E. & Casasent, D. A comparison between criterion functions for linear classifiers, with an application to neural nets. *IEEE Transactions On Systems, Man, And Cybernetics*. **19**, 1030-1041 (1989), DOI: 10.1109/21.44018
- [135] Mikolajczyk, A. & Grochowski, M. Data augmentation for improving deep learning in image classification problem. *2018 International Interdisciplinary PhD Workshop (IIPhDW)*. pp. 117-122 (2018), DOI: 10.1109/IIPHDW.2018.8388338, ISBN: 978-1-5386-6143-7
- [136] GoogleAI Responsible AI practices. (<https://ai.google/responsibilities/responsible-ai-practices?category=general>), Accessed: 2022-05-14
- [137] Tajudin, A., Sulaiman, S., Isa, I., Soh, Z., Karim, N. & Shuaib, I. Microbleeds detection using watershed-driven active contour. *2017 7th IEEE International Conference On Control System, Computing And Engineering (ICCSC)*. pp. 320-324 (2017), DOI: 10.1109/ICCSC.2017.8284427, ISBN: 978-1-5386-3897-2
- [138] Afzal, S., Khan, I. & Lee, J. A Transfer Learning-Based Approach to Detect Cerebral Microbleeds. *Computers, Materials & Continua*. **71**, 1903 (2022), DOI: 10.32604/cmc.2022.021930, ISSN: 1546-2218
- [139] Tao, Y. & Cloutie, R. Voxelwise Detection of Cerebral Microbleed in CADASIL Patients by Genetic Algorithm and Back Propagation Neural Network. *Proceedings Of The 2018 3rd International Conference On Communications, Information Management And Network Security (CIMNS 2018)*. (2018), DOI: 10.2991/cimns-18.2018.23, ISBN: 978-94-6252-620-4
- [140] Standvoss, K., Crijs, T., Goerke, L., Janssen, D., Kern, S., Niedek, T., Vugt, J., Burgos, N., Gerritse, E., Mol, J., Vooren, D., Ghafoorian, M., Heuvel, T. & Manniesing, R. Cerebral microbleed detection in traumatic brain injury patients using 3D convolutional neural networks. *Medical Imaging 2018: Computer-Aided Diagnosis*. **10575** pp. 314 - 321 (2018), DOI: 10.1117/12.2294016
- [141] Creswell, A., White, T., Dumoulin, V., Arulkumaran, K., Sengupta, B. & Bharath, A. Generative Adversarial Networks: An Overview. *IEEE Signal Processing Magazine*. **35**, 53-65 (2018), DOI: 10.1109/MSP.2017.2765202, ISSN: 1053-5888
- [142] The Precise4Q consortium, Amann, J., Blasimme, A., Vayena, E., Frey, D. & Madai, V. Explainability for artificial intelligence in healthcare: a multidisciplinary perspective. *BMC Medical Informatics And Decision Making*. **20**, 310 (2020), DOI: 10.1186/s12911-020-01332-6, ISSN: 1472-6947
- [143] Barredo Arrieta, A., Díaz-Rodríguez, N., Del Ser, J., Bennetot, A., Tabik, S., Barbado, A., Garcia, S., Gil-Lopez, S., Molina, D., Benjamins, R., Chatila, R. & Herrera, F. Explainable Artificial Intelligence (XAI): Concepts, taxonomies, opportunities and challenges toward responsible AI. *Information Fusion*. **58** pp. 82-115 (2020), DOI: 10.1016/j.inffus.2019.12.012, ISSN: 1566-2535
- [144] Angelov, P., Soares, E., Jiang, R., Arnold, N. & Atkinson, P. Explainable artificial intelligence: an analytical review. *WIREs Data Mining And Knowledge Discovery*. **11** (2021), DOI: 10.1002/widm.1424, ISSN: 1942-4787, 1942-4795
- [145] Mikolajczyk, A., Grochowski, M. & Kwasigroch, A. Towards Explainable Classifiers Using the Counterfactual Approach - Global Explanations for Discovering Bias in Data. *Journal Of Artificial Intelligence And Soft Computing Research*. **11**, 51-67 (2021), DOI: 10.2478/jaiscr-2021-0004, ISSN: 2083-2567
- [146] Leming, M., Das, S. & Im, H. Construction of a confounder-free clinical MRI dataset in the Mass General Brigham system for classification of Alzheimer's disease. *Artificial Intelligence In Medicine*. **129** pp. 102309 (2022), DOI: 10.1016/j.artmed.2022.102309, ISSN: 09333657
- [147] Currie, S., Hoggard, N., Craven, I., Hadjivassiliou, M. & Wilkinson, I. Understanding MRI: basic MR physics for physicians. *Postgraduate Medical Journal*. **89**, 209-223 (2013), DOI: 10.1136/postgradmedj-2012-131342, ISSN: 0032-5473, 1469-0756
- [148] Poels, M., Ikram, M., Lugt, A., Hofman, A., Krestin, G., Breteler, M. & Vernooij, M. Incidence of Cerebral Microbleeds in the General Population. *Stroke*. **42**, 656-661 (2011), DOI: 10.1161/STROKEAHA.110.607184
- [149] Nusrat, I. & Jang, S. A Comparison of Regularization Techniques in Deep Neural Networks. *Symmetry*. **10**, 648 (2018), DOI:10.3390/sym10110648, ISSN:2073-8994
- [150] Jain, A. & Ramaswami, M. Classifier Design with Parzen Windows. *Pattern Recognition And Artificial Intelligence*. **7** pp. 211-228 (1988), DOI:10.1016/B978-0-444-87137-4.50021-7, ISSN: 0923-0459
- [151] Tharwat, A. Linear vs. quadratic discriminant analysis classifier: a tutorial. *International Journal Of Applied Pattern Recognition*. **3**, 145 (2016), DOI:10.1504/IJAPR.2016.079050, ISSN: 2049-887X, 2049-8888

- [152] Comon, P. Supervised classification: a probabilistic approach. *ESANN95-European Symposium On Artificial Neural Networks*. pp. 111-128 (1995)
- [153] Averbuch, A. & Shkolnisky, Y. 3D Fourier based discrete Radon transform. *Applied And Computational Harmonic Analysis*. **15**, 33-69 (2003), DOI:10.1016/S1063-5203(03)00030-7, ISSN: 1063-5203
- [154] Luo, L., Ye, L., Luo, M., Huang, D., Peng, H. & Yang, F. Methods of forward feature selection based on the aggregation of classifiers generated by single attribute. *Computers In Biology And Medicine*. **41**, 435-441 (2011), DOI:10.1016/j.compbiomed.2011.04.005, ISSN: 00104825
- [155] Wang, S. Artificial Neural Network. *Interdisciplinary Computing In Java Programming*. pp. 81-100 (2003), DOI: 10.1007/978-1-4615-0377-4\_5, ISBN: 978-1-4615-0377-4
- [156] Al., U. The RSNA-ASNR-MICCAI BraTS 2021 Benchmark on Brain Tumor Segmentation and Radiogenomic Classification. *ArXiv*. (2021), Number: arXiv:2107.02314, arXiv:2107.02314 [cs]
- [157] Siegel, E. What Can We Learn from the RSNA Pediatric Bone Age Machine Learning Challenge?. *Radiology*. **290**, 504-505 (2019), DOI: 10.1148/radiol.2018182657, ISSN: 0033-8419, 1527-1315
- [158] Halabi, S., Prevedello, L., Kalpathy-Cramer, J., Mamonov, A., Bilbily, A., Cicero, M., Pan, I., Pereira, L., Sousa, R., Abdala, N., Kitamura, F., Thodberg, H., Chen, L., Shih, G., Andriole, K., Kohli, M., Erickson, B. & Flanders, A. The RSNA Pediatric Bone Age Machine Learning Challenge. *Radiology*. **290**, 498-503 (2019), DOI: 10.1148/radiol.2018180736, ISSN: 0033-8419, 1527-1315
- [159] Pinykh, O., Lings, G., Dewey, M., Enzmann, D., Herold, C., Schoenberg, S. & Brink, J. Continuous Learning AI in Radiology: Implementation Principles and Early Applications. *Radiology*. **297**, 6-14 (2020), DOI: 10.1148/radiol.2020200038, ISSN:0033-8419, 1527-1315
- [160] Sveinbjornsdottir, S., Sigurdsson, S., Aspelund, T., Kjartansson, O., Eiriksdottir, G., Valtysdottir, B., Lopez, O., Buchem, M., Jonsson, P., Gudnason, V. & Launer, L. Cerebral microbleeds in the population based AGES-Reykjavik study: prevalence and location. *Journal Of Neurology, Neurosurgery & Psychiatry*. **79**, 1002 (2008)
- [161] Werring, D. Cognitive dysfunction in patients with cerebral microbleeds on T2\*-weighted gradient-echo MRI. *Brain*. **127**, 2265-2275 (2004), DOI: 10.1093/brain/awh253, ISSN: 1460-2156
- [162] Poels, M., Ikram, M., Lugt, A., Hofman, A., Niessen, W., Krestin, G., Breteler, M. & Vernooij, M. Cerebral microbleeds are associated with worse cognitive function. *Neurology*. **78**, 326 (2012), DOI: 10.1212/WNL.0b013e3182452928
- [163] Cordonnier, C. & Flier, W. Brain microbleeds and Alzheimer's disease: innocent observation or key player?. *Brain*. **134**, 335-344 (2011), DOI: 10.1093/brain/awq321, ISSN: 1460-2156, 0006-8950
- [164] Bian, W., Hess, C., Chang, S., Nelson, S. & Lupo, J. Susceptibility-weighted MR imaging of radiation therapy-induced cerebral microbleeds in patients with glioma: a comparison between 3T and 7T. *Neuroradiology*. **56**, 91-96 (2014), DOI: 10.1007/s00234-013-1297-8, ISSN: 0028-3940, 1432-1920
- [165] Revol-Muller, C., Peyrin, F., Carrillon, Y. & Odet, C. Automated 3D region growing algorithm based on an assessment function. *Pattern Recognition Letters*. **23**, 137-150 (2002), DOI: 10.1016/S0167-8655(01)00116-7, ISSN: 01678655
- [166] Buscema, M. Back Propagation Neural Networks. *Substance Use & Misuse*. **33**, 233-270 (1998,1), DOI: 10.3109/10826089809115863, ISSN: 1082-6084, 1532-2491
- [167] Lee, H., Battle, A., Raina, R. & Ng, A. Efficient sparse coding algorithms. *Advances In Neural Information Processing Systems 19*. pp. 8 (2006)
- [168] O'Shea, K. & Nash, R. An Introduction to Convolutional Neural Networks. (arXiv,2015), Number: arXiv:1511.08458 [cs]
- [169] Singh, S., Wang, L., Gupta, S., Goli, H., Padmanabhan, P. & Gulyás, B. 3D Deep Learning on Medical Images: A Review. *Sensors*. **20**, 5097 (2020), DOI: 10.3390/s20185097, ISSN: 1424-8220
- [170] Haller, S., Haacke, E., Thurnher, M. & Barkhof, F. Susceptibility-weighted Imaging: Technical Essentials and Clinical Neurologic Applications. *Radiology*. **299**, 3-26 (2021,4), ISSN: 0033-8419, 1527-1315, DOI: 10.1148/radiol.2021203071
- [171] Hodel, J., Rodallec, M., Gerber, S., Blanc, R., Maraval, A., Caron, S., Tyvaert, L., Zuber, M. & Zins, M. Séquences IRM SWAN, SWI et VenoBOLD exploitant le phénomène de susceptibilité magnétique : principes techniques et applications cliniques. *Journal Of Neuroradiology*. **39**, 71-86 (2012,5,1), ISSN: 0150-9861, DOI: 10.1016/j.neurad.2011.11.006, language: French

- [172] Nandigam, K. & Scully, M. SWAN MRI revealing multiple microhemorrhages secondary to septic emboli from mucormycosis. *Neurology*. **81**, 199-200 (2013,7,9), ISSN: 0028-3878, 1526-632X, DOI: 10.1212/01.wnl.0000432237.13307.12
- [173] Ayaz, M., Boikov, A., Haacke, E., Kido, D. & Kirsch, W. Imaging cerebral microbleeds using susceptibility weighted imaging: one step toward detecting vascular dementia. *Journal Of Magnetic Resonance Imaging: JMRI*. **31**, 142-148 (2010), ISSN: 1522-2586, DOI: 10.1002/jmri.22001
- [174] Haller, S., Vernooij, M., Kuijter, J., Larsson, E., Jäger, H. & Barkhof, F. Cerebral Microbleeds: Imaging and Clinical Significance. *Radiology*. **287**, 11-28 (2018), DOI: 10.1148/radiol.2018170803, ISSN: 0033-8419